Article

Cell Reports

A Fatty Acid Oxidation-Dependent Metabolic Shift Regulates Adult Neural Stem Cell Activity

Graphical Abstract

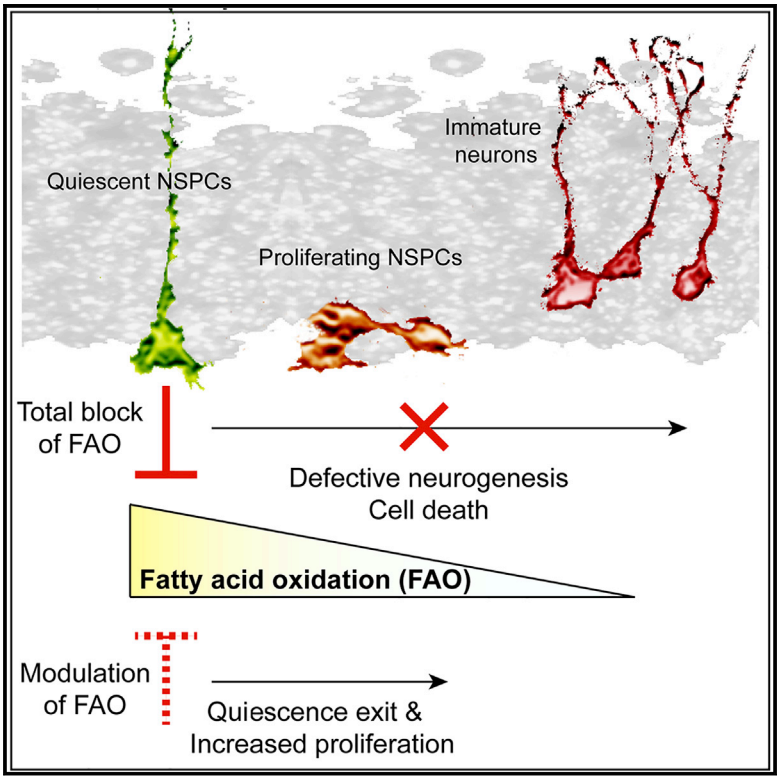

Highlights

- A metabolic shift defines NSPC quiescence versus proliferation
- Quiescent NSPCs require high levels of FAO
- Changing levels of a single metabolite is sufficient to induce NSPC proliferation

Authors

Marlen Knobloch, Gregor-Alexander Pilz, Bart Ghesquière, ..., Nicola Zamboni, Peter Carmeliet, Sebastian Jessberger

Correspondence

marlen.knobloch@unil.ch (M.K.), jessberger@hifo.uzh.ch (S.J.)

In Brief

Controlled balance between proliferation and quiescence of neural stem/progenitor cells (NSPCs) is required for lifelong neurogenesis. Knobloch et al. identify a metabolic shift in fatty acid oxidation (FAO) that governs the proliferation of NSPCs. Further, their data suggest an instructive role for FAO in regulating NSPC activity. Thus, Knobloch et al. identify FAO as a key metabolic pathway to regulate NSPC activity.

Knobloch et al., 2017, Cell Reports *20*, 2144–2155
August 29, 2017 © 2017 The Author(s).
http://dx.doi.org/10.1016/j.celrep.2017.08.029

CellPress

OPEN ACCESS
CellPress

Cell Reports
Article

A Fatty Acid Oxidation-Dependent Metabolic Shift Regulates Adult Neural Stem Cell Activity

Marlen Knobloch,[1,7,*] Gregor-Alexander Pilz,[1] Bart Ghesquière,[2,3] Werner J. Kovacs,[4] Thomas Wegleiter,[1] Darcie L. Moore,[1] Martina Hruzova,[1] Nicola Zamboni,[5] Peter Carmeliet,[3,6] and Sebastian Jessberger[1,8,*]

[1]Laboratory of Neural Plasticity, Faculty of Medicine and Science, Brain Research Institute, University of Zurich, 8057 Zurich, Switzerland
[2]VIB Metabolomics Expertise Center, 3000 Leuven, Belgium
[3]Laboratory of Angiogenesis & Vascular Metabolism, Vesalius Research Center VIB, 3000 Leuven, Belgium
[4]Institute of Molecular Health Sciences, Department of Biology, ETH Zurich, 8093 Zurich, Switzerland
[5]Institute of Molecular Systems Biology, Department of Biology, ETH Zurich, 8093 Zurich, Switzerland
[6]Laboratory of Angiogenesis & Vascular Metabolism, Department of Oncology, KU Leuven, 3000 Leuven, Belgium
[7]Present address: Department of Physiology, University of Lausanne, 1005 Lausanne, Switzerland
[8]Lead Contact
*Correspondence: marlen.knobloch@unil.ch (M.K.), jessberger@hifo.uzh.ch (S.J.)
http://dx.doi.org/10.1016/j.celrep.2017.08.029

SUMMARY

Hippocampal neurogenesis is important for certain forms of cognition, and failing neurogenesis has been implicated in neuropsychiatric diseases. The neurogenic capacity of hippocampal neural stem/progenitor cells (NSPCs) depends on a balance between quiescent and proliferative states. Here, we show that the rate of fatty acid oxidation (FAO) regulates the activity of NSPCs. Quiescent NSPCs show high levels of carnitine palmitoyltransferase 1a (Cpt1a)-dependent FAO, which is downregulated in proliferating NSPCs. Pharmacological inhibition and conditional deletion of Cpt1a in vitro and in vivo leads to altered NSPC behavior, showing that Cpt1a-dependent FAO is required for stem cell maintenance and proper neurogenesis. Strikingly, manipulation of malonyl-CoA, the metabolite that regulates levels of FAO, is sufficient to induce exit from quiescence and to enhance NSPC proliferation. Thus, the data presented here identify a shift in FAO metabolism that governs NSPC behavior and suggest an instructive role for fatty acid metabolism in regulating NSPC activity.

INTRODUCTION

New neurons are generated throughout life in the mammalian hippocampus (Spalding et al., 2013; van Praag et al., 2002). This process, called adult neurogenesis, is critically involved in a variety of hippocampus-dependent forms of learning and memory (Clelland et al., 2009; Deng et al., 2010; Dupret et al., 2008; Gonçalves et al., 2016; Nakashiba et al., 2012; Sahay et al., 2011a, 2011b). In addition, failing or altered neurogenesis has been associated with a number of neuropsychiatric diseases, such as major depression, epilepsy, and cognitive aging, suggesting adult hippocampal neurogenesis is relevant for human health and disease (Christian et al., 2014; Kempermann et al., 2008; Scharfman and Hen, 2007). Neural stem/progenitor cells (NSPCs) in the adult hippocampus reside in the subgranular zone (SGZ) of the dentate gyrus (DG), where they proliferate and generate new glutamatergic, excitatory granule cells that become integrated into pre-existing circuitries over the course of several weeks (Espósito et al., 2005; Ge et al., 2007; Lagace et al., 2007; Seri et al., 2001; Toni et al., 2008; Zhao et al., 2006). Previous reports have suggested a delicate balance between quiescent, radial glia-like NSPCs and more proliferative NSPCs controlled by key signaling pathways, such as Notch and BMP signaling, resembling molecular mechanisms identified in the developing brain (Ables et al., 2010; Ehm et al., 2010; Lugert et al., 2010; Ming and Song, 2011; Mira et al., 2010). In addition, accumulating evidence in NSPCs and other somatic stem cells, such as hematopoietic stem cells (HSCs), has suggested that cellular metabolism might govern the levels of activity of adult stem cells in vivo and during cellular reprogramming in vitro (Chorna et al., 2013; David, 2011; Folmes et al., 2011; Homem et al., 2015; Ito et al., 2012; Ito and Suda, 2014; Knobloch et al., 2013; Ryall et al., 2015). However, whether specific metabolic programs regulate the balance between NSPC quiescence and proliferation remains unknown. The brain is the organ with the highest glucose consumption rate (Mergenthaler et al., 2013), and neurons are mainly dependent on glucose and lactate for normal function. The role of lipids in brain metabolism has been much less studied, given the predominance of glucose consumption. Furthermore, the relatively small proportion of NSPCs compared to the cellular mass of the brain might have led to the overlooking of other metabolic pathways relevant for NSPCs. Indeed, we have previously identified an important role for lipid metabolism in NSPCs, showing that the build-up of lipids through de novo lipogenesis is crucial for proliferation (Knobloch et al., 2013). However, whether the metabolic counterpart, the breakdown of lipids called fatty acid oxidation (FAO), is important to regulate NSPC behavior remains poorly understood. We here characterized metabolic adaptations from a quiescent to an activated NSPC state and identified FAO as a key metabolic pathway to regulate NSPC quiescence.

 © 2017 The Author(s).
This is an open access article under the CC BY-NC-ND license (http://creativecommons.org/licenses/by-nc-nd/4.0/).

RESULTS

Quiescent NSPCs Have High Levels of FAO

To study metabolic adaptations during NSPC quiescence versus activation, we modified previously established in vitro protocols that are based on the induction of NSPC quiescence by bone morphogenic protein 4 (BMP4), leading to cellular quiescence over the course of three days (Figure 1A) (Martynoga et al., 2013; Mira et al., 2010). BMP4-induced quiescence was reversible with restored proliferation and differentiation potential after removal of quiescence cues, suggesting a reliable in vitro model of functional NSPC quiescence (Figures S1A–S1C). We first analyzed the whole proteome of proliferating compared to quiescent NSPCs and found proteins associated with FAO (the breakdown of fatty acids into acetyl-coenzyme A [CoA] in the mitochondria) to be highly enriched in quiescent NSPCs (Figures 1B and S1D–S1F; Tables S1 and S2). To test whether the high expression levels of proteins associated with FAO translate into functionally elevated levels of FAO, we used radioactive FAO measurements. A labeled fatty acid (^{3}H-palmitic acid) was added to the medium. During oxidation of such labeled palmitic acid into eight acetyl-CoAs, measurable radioactive labeled water (^3H_2O) is produced, which serves as a readout of the rate of FAO. Strikingly, we found high levels of FAO in quiescent NSPCs that were substantially lower in proliferating NSPCs (Figure 1C).

To characterize FAO in quiescent NSPCs, we analyzed the expression of carnitine palmitoyltransferase 1a (Cpt1a), a rate-limiting mitochondrial enzyme of FAO that mediates the transport of fatty acids into the mitochondria (Houten and Wanders, 2010). Corroborating the proteomics data, we found strong upregulation of Cpt1a using qRT-PCR and western blot analyses, showing a substantial increase in the expression of Cpt1a in quiescent compared to proliferating NSPCs (Figures 1D and 1E). In line with the radioactive FAO measurements, the increase in Cpt1a expression in quiescent NSPCs was reversible (Figure 1D). Cpt1a co-labeled with the mitochondrial dye Mitotracker in both quiescent and proliferating NSPCs (Figures 1H and S1H). In addition, Cpt1a was highly expressed in NSPCs compared to their neuronal progeny when directly isolated from the adult DG (3.5-fold upregulated in SOX2+ cells versus DCX+ cells), as described previously (Bracko et al., 2012; Shin et al., 2015). Collectively, these data indicate that compared to proliferating NSPCs that are highly lipogenic (Knobloch et al., 2013), quiescent NSPCs strongly express Cpt1a and show high levels of functional FAO.

Next, we aimed to understand the molecular mechanism underlying high levels of FAO in quiescent NSPCs. We have previously shown that Spot14 is selectively expressed in quiescent NSPCs in vivo (Knobloch et al., 2013, 2014). When we induced quiescence in vitro, we found a >30-fold upregulation of Spot14 mRNA using qRT-PCR (Figure 1F). Given that Spot14 negatively regulates malonyl-CoA levels (Colbert et al., 2010; Knobloch et al., 2013), we expected that high levels of Spot14 in quiescent NSPCs would lead to low levels of malonyl-CoA. Indeed, quiescent NSPCs showed a substantial decrease in malonyl-CoA, as measured with mass spectrometry (Figure 1G). The levels of acetyl-CoA, which are not affected by Spot14, were comparable between proliferating and quiescent NSPCs (Figure S1G). Because malonyl-CoA is an endogenous inhibitor of Cpt1a, its levels determine the rate of FAO (Folmes et al., 2013; Houten and Wanders, 2010). Thus, high levels of Spot14 accompanied by low levels of malonyl-CoA in quiescent NSPCs promote high FAO (see also summary scheme Figure 5E).

High Levels of FAO Are Required to Sustain Cellular Quiescence

To test for the functional relevance of FAO activity, we blocked FAO in quiescent NSPCs using the irreversible Cpt1 inhibitor Etomoxir. NSPCs were induced to quiescence and then exposed to various doses of Etomoxir. Cell survival was assessed using time-lapse imaging. Strikingly, such complete FAO inhibition in quiescent NSPCs led to massive cell death in a dose-dependent manner (Figure 2A). This finding indicates that FAO is critically involved in maintaining adult hippocampal NSPCs in a quiescent state and that absence of this pathway is detrimental. Complete blockage of FAO using Etomoxir also affected NSPCs kept under proliferating conditions by reducing their proliferation, as assessed by time-lapse imaging, flow cytometry analysis, and 5-ethynyl-2'-deoxyuridine (EdU)-pulse labeling (Figures S2A–S2C). These findings are in line with a recent report showing that proliferating NSPCs in the SVZ can oxidize fatty acids (Stoll et al., 2015). Given the detectable levels of FAO in proliferating NSPCs, (although much lower than in quiescent NSPCs; Figure 1C) and the effect of blocking FAO on proliferation, these data suggest that FAO is still to a certain extend relevant during proliferation. However, in contrast to quiescent NSPCs, abolishing FAO in proliferating NSPCs only mildly affected their cell survival (Figures S2A–S2C).

Given the importance of FAO for NSPC behavior in vitro, we next investigated why quiescent NSPCs require FAO. We used two complementary approaches to analyze the fate of oxidized fatty acids in NSPCs. First, we used radioactively labeled ^{14}C-palmitic acid to determine the complete oxidation of fatty acids, allowing for energy production. In contrast to the ^{3}H-palmitic acid labeling, where radioactive labeled ^3H_2O is produced during the entire oxidation cycles into acetyl-CoAs, radioactively labeled ^{14}C-palmitic acid yields measureable $^{14}CO_2$ only if the resulting acetyl-CoAs are further oxidized in the tricarboxylic acid (TCA) cycle. We found significantly higher levels of $^{14}CO_2$ in quiescent NSPCs compared to proliferating NSPCs, suggesting that quiescent NSPCs might use fatty acids as a fuel source (Figure 2B). To confirm that quiescent NSPCs use FAO for energy production, we determined their energy charge, as a readout for the amount of energy available in the form of adenosine triphosphate (ATP). We found that the energy charge significantly dropped following Etomoxir treatment, indicating that FAO is indeed contributing to the amount of ATP generated in quiescent NSPCs (Figure 2C), with the massive drop using 200 μm Etomoxir probably indicating reduced cell viability.

Next, we used ^{13}C-labeled palmitic acid to trace the incorporation of labeled carbon atoms in quiescent versus proliferative NSPCs (Figure 2D). During complete oxidation of such labeled palmitic acid, labeled carbon atoms are cleaved off and transferred to TCA intermediates and amino acids derived from TCA intermediates. The amount of incorporation of labeled carbons

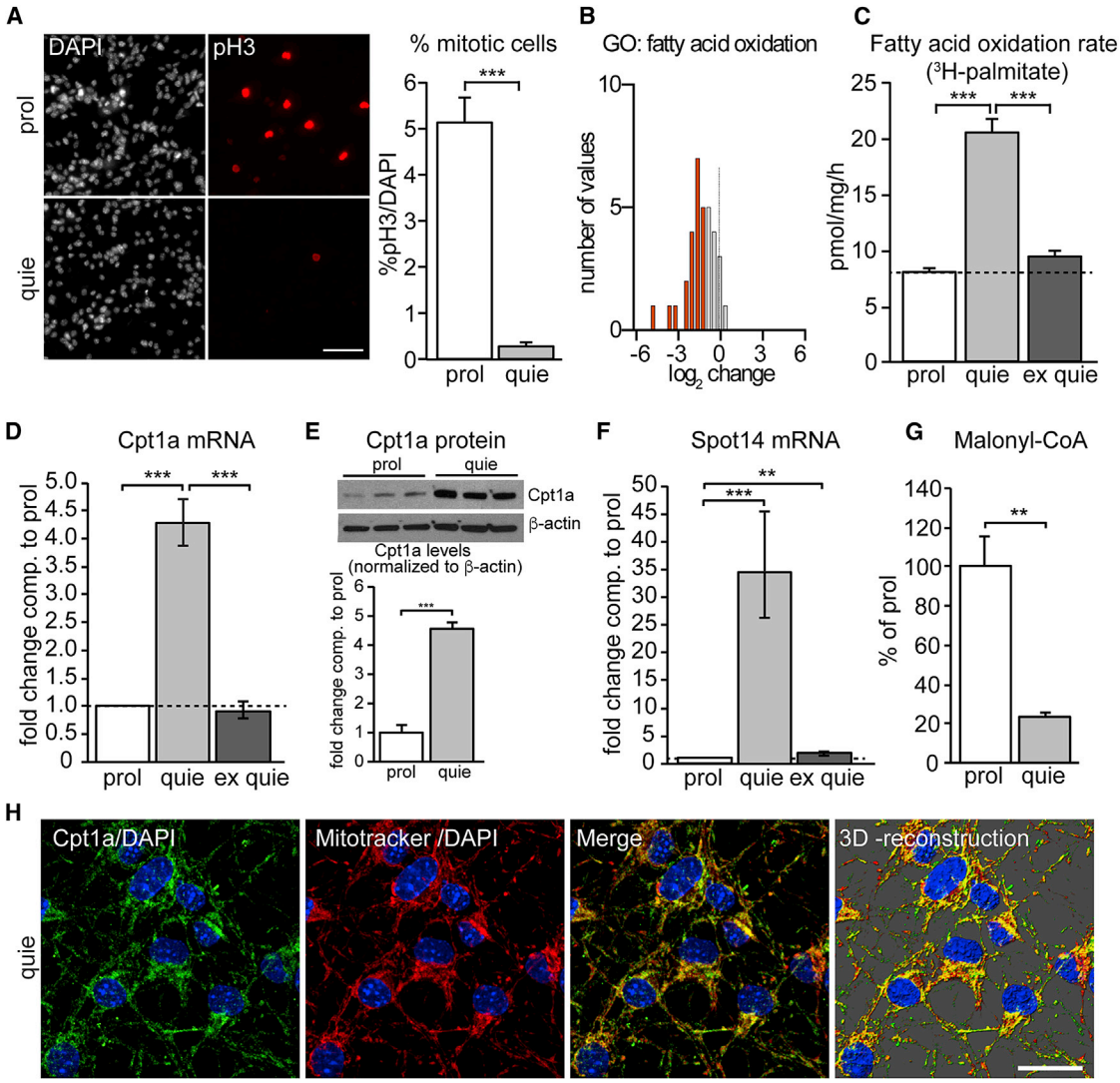

Figure 1. Quiescent NSPCs Have a High Rate of FAO

(A) Exposure of NSPCs to a BMP4-containing quiescence medium for three days leads to a massive decrease in proliferation. Shown are representative images of proliferating (prol) and quiescent (quie) NSPCs and quantification of the mitotic cell marker phospho histone 3 (pH3) (mean ± SEM).

(B) Mass spectrometric comparison of the proteome of proliferating and quiescent NSPCs reveals FAO to be enriched in quiescent NSPCs. The histogram shows the normalized abundance of proteins belonging to the GO term "Fatty acid oxidation" (gray = expression change of $\log_2 < |1|$, red = expression change of $\log_2 \leq -1$, enriched in quiescent cells).

(C) Radioactive FAO measurements using ^{3}H-labeled palmitic acid revealed a significant increase in the rate of FAO in quiescent NSPCs compared to proliferating NSPCs. Remarkably, this increase was reversed in quiescent NSPCs that had been re-exposed to proliferation conditions (ex quie), suggesting FAO is specifically upregulated upon quiescence entry (mean ± SD).

(D) mRNA levels of the key FAO enzyme Cpt1a are highly and reversibly upregulated in quiescent (quie) NSPCs compared to proliferating (prol) and formerly quiescent (ex quie) NSPCs (mean ± SEM).

(E) The increase in Cpt1a mRNA levels is also reflected on protein levels, as revealed by western blot analysis (mean ± SEM).

(F) mRNA levels of the previously described novel quiescence marker Spot14 are highly upregulated in quiescent (quie) NSPCs compared to proliferating (prol) NSPCs. This upregulation is reversible, as formerly quiescent (ex quie) NSPCs greatly reduce Spot14 mRNA levels. This suggests that the BMP4-induced in vitro quiescence system indeed reflects features of in vivo NSPC quiescence (mean ± SEM).

(G) The endogenous Cpt1a inhibitor malonyl-CoA is lowered in quiescent NSPCs compared to proliferating NSPCs, as measured by mass spectrometry analysis (mean ± SEM).

(H) Co-stainings against Cpt1a and a mitochondrial marker (Mitotracker) reveals the mitochondrial localization of Cpt1a in quiescent NSPCs. Shown is a representative confocal image of maximum projections of individual channels and a 3D reconstruction.

Scale bars represent 50 μm (A) and 20 μm (H). ***$p < 0.001$; **$p < 0.01$.

See also Figure S1.

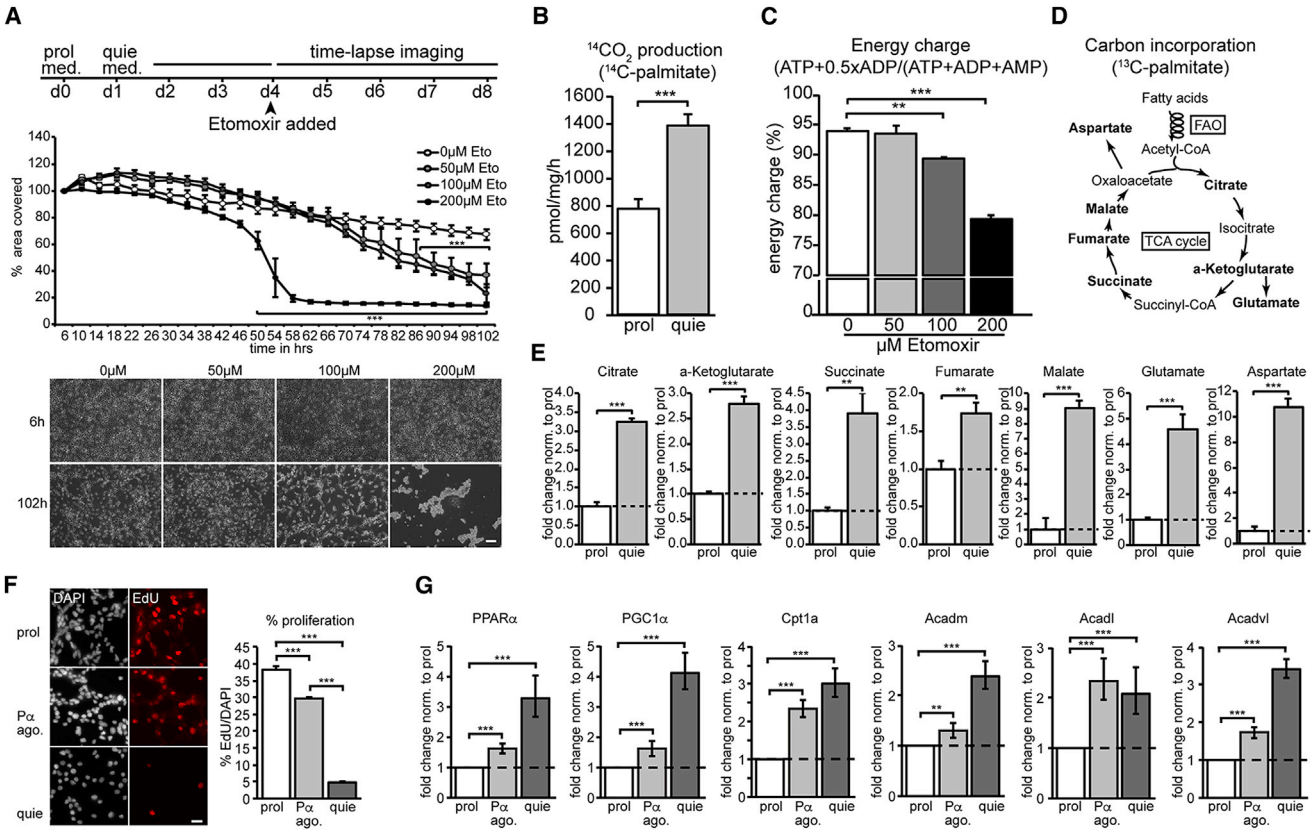

Figure 2. High Levels of FAO Are Required to Sustain Cellular Quiescence

(A) Time-lapse analysis of quiescent NSPCs exposed to various doses of the irreversible Cpt1 inhibitor Etomoxir (50, 100, and 200 μM). Shown are a schematic outline of the experimental setup, the quantification of the area covered by quiescent NSPCs over time, and representative images. Complete block of FAO by Etomoxir during quiescence leads to a dramatic and dose-dependent decrease of area covered over time, caused by cell death upon FAO inhibition (mean ± SEM).

(B–E) Quiescent NSPCs use FAO for energy purposes and may use it as an alternative carbon source.

(B) Radioactive FAO measurements using ^{14}C-labeled palmitic acid revealed a significant increase in $^{14}CO_2$ in quiescent NSPCs compared to proliferating NSPCs, suggesting that at least part of the fatty acids are fully oxidized and might be used for energy purposes (mean ± SD).

(C) Energy charge measurements in quiescent NSPCs show that FAO indeed contributes to the amount of ATP generated, as treatment with various doses of Etomoxir (50, 100, and 200 μM) reduced the energy charge significantly (mean ± SEM).

(D) Scheme outlining the path of ^{13}C-labeled palmitic acid upon FAO. The oxidation of fatty acids results in acetyl-CoA, which can be fed into the TCA. The metabolites measured with mass spectrometry in a ^{13}C-incorporation assay are shown in bold.

(E) Quiescent NSPCs show an increase in ^{13}C-incorporation in TCA intermediates and amino acids derived from TCA intermediates compared to proliferating NSPCs (mean ± SD). These ^{13}C-incorporation assay results suggest that fatty acids might also serve as an alternative carbon source in quiescent NSPCs.

(F) High levels of FAO in quiescent NSPCs are at least partially regulated through the transcription factor PPARα. Treatment for 48 hr with 100 μM of the PPARα agonist WY14643 in proliferating NSPCs significantly reduced proliferation compared to control NSPCs, but proliferation was still far higher than in quiescent NSPCs, as assessed by EdU pulsing. Shown are representative images and the corresponding quantification of EdU-positive cells (mean ± SEM).

(G) WY14643 treatment led to an upregulation of PPARα and its target FAO genes in proliferating NSPCs compared to control NSPCs, however, to a far lesser extent than in quiescent NSPCs. Shown are the mRNA expression levels (mean fold change ± range) of PPARα, Peroxisome proliferator-activated receptor gamma coactivator 1-alpha (PGC1α), Cpt1a, medium-chain acyl-CoA dehydrogenase (Acadm), long-chain acyl-CoA dehydrogenase (Acadl), and very long-chain acyl-CoA dehydrogenase (Acadvl).

Scale bar represents 50 μm (A) and 20 μm (F). ***p < 0.001; **p < 0.01.

See also Figure S2 and Table S3.

can be measured using mass spectrometry. We found highly significant increases in the incorporation of ^{13}C into TCA intermediates as well as into amino acids derived from TCA intermediates in quiescent NSPCs (Figure 2E), suggesting that the fatty acid-derived carbon atoms might be further used as an alternative carbon source.

To address whether the upregulation of FAO in quiescent NSPCs is transcriptionally regulated, we measured the expression levels of the Peroxisome proliferator-activated receptor alpha (PPARα), a known transcriptional regulator of genes involved in FAO by qRT-PCR (Leone et al., 1999). Indeed, expression of PPARα and its target genes was highly upregulated in quiescent NSPCs compared to proliferating NSPCs (Figures 2G and S2D), suggesting that upregulation of FAO upon quiescence is at least partially regulated on a transcriptional level. Given this transcriptional component of FAO regulation

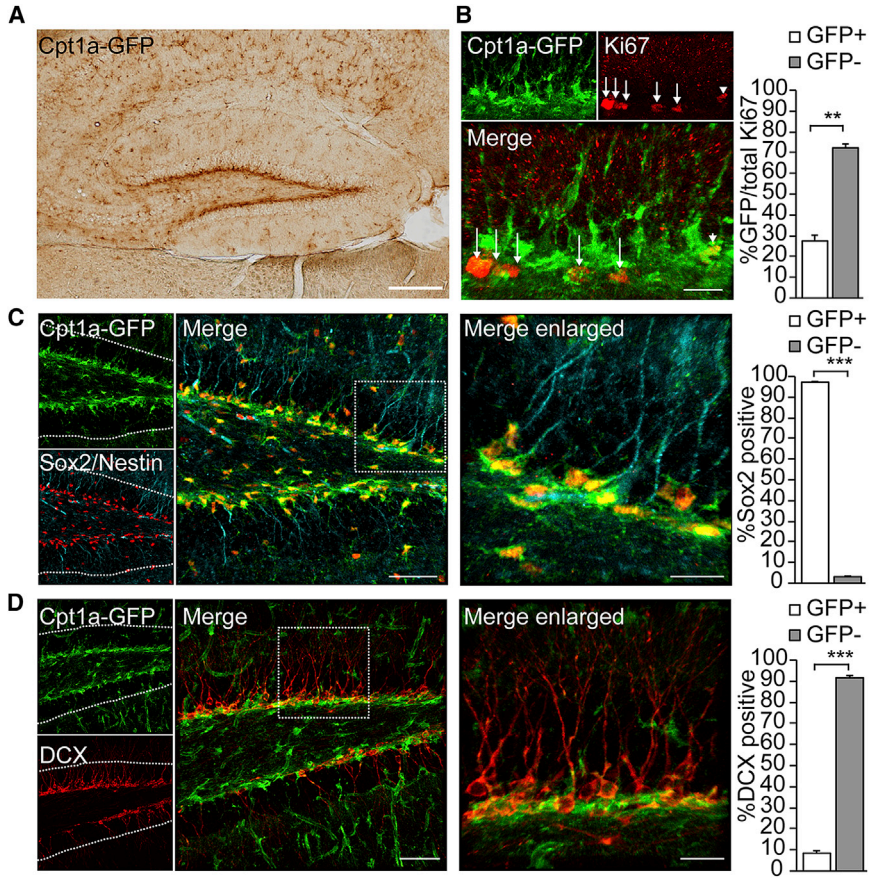

Figure 3. Cpt1a Is Expressed in Adult NSPCs In Vivo

(A) Immunohistological analysis of a reporter mouse expressing GFP under the Cpt1a promoter reveals high GFP expression in the SGZ of the DG, where NSPCs reside. Shown is a representative image of a brain section from a 2-month-old animal.

(B) Co-stainings for Cpt1a-GFP and the proliferation marker Ki67 show that the majority of proliferating NSPCs do not express GFP, supporting the findings that FAO is specifically upregulated in quiescent NSPCs. Shown is a representative confocal image (maximum projection) from a 2-month-old Cpt1a-GFP reporter mouse. Arrows indicate Ki67+/GFP− cells; the arrowhead points to a Ki67+/GFP+ cell. The bar graph shows the percentage of GFP+ and GFP− NSPCs out of all Ki67+ cells in the SGZ of the DG (mean ± SEM).

(C) Cpt1a-GFP-positive NSPCs are almost all positive for the NSPC marker SOX2, and GFP+ processes co-stain with the NSPC marker Nestin. Shown is a representative confocal image (maximum projection) from a 2-month-old Cpt1a-GFP reporter mouse. Dotted lines show the outline of the granular zone of the DG, the boxed area is enlarged in the right panel. The bar graph shows the percentage of GFP+ and GFP− NSPCs out of SOX2+ cells (mean ± SEM).

(D) Cpt1a-GFP-positive NSPCs are almost all negative for the immature neuronal marker Doublecortin (DCX), suggesting that FAO is downregulated upon neuronal lineage commitment. Shown is a representative confocal image (maximum projection) from a 2-month-old Cpt1a-GFP reporter mouse. Dotted lines show the outline of the granular zone of the DG, the boxed area is enlarged in the right panel. The bar graph shows the percentage of GFP+ and GFP− NSPCs out of DCX+ cells (mean ± SEM).

Scale bars represent 200 μm (A), 50 μm (C and D, left), and 20 μm (B, C, and D, right).

See also Figure S3.

through PPARα, we next assessed whether FAO gene expression could be modulated in proliferating NSPCs to reach similar levels as in quiescent NSPCs and whether such an upregulation would render proliferating NSPCs more quiescent. Treatment with the PPARα agonist WY14643 indeed led to an upregulation of FAO genes in proliferating NSPCs compared to control NSPCs (Figure 2G and S2D), however, to a far lesser extent than in quiescent NSPCs. Similarly, although modulation of FAO genes by WY14643 significantly reduced proliferation compared to control NSPCs, proliferation was still far higher than in quiescent NSPCs (Figure 2F).

Cpt1a Is Expressed in Hippocampal NSPCs In Vivo

After identifying a role for FAO in NSPC quiescence in vitro, we next analyzed the expression of Cpt1a within the adult hippocampal neurogenic niche using a Cpt1a reporter mouse expressing GFP from the regulatory elements of the Cpt1a genomic locus (Genesat; hereafter called Cpt1a-GFP) (Gong et al., 2003). Besides GFP-positive classical astrocytes throughout all hippocampal subfields (Figures 3A and S3B), we found GFP expression to be highly enriched in the subgranular zone (SGZ) of the DG (Figures 3A and S3A). GFP-positive cells expressed Cpt1a, as confirmed with staining against endogenous Cpt1a (Figure S3C). Next, we phenotyped GFP-labeled cells in Cpt1a-GFP mice and found that GFP expression preferentially labeled non-mitotic, Ki67-negative hippocampal NSPCs and only a small subset of cycling NSPCs (Figure 3B). Virtually all Cpt1a-GFP-positive cells co-labeled with the radial and non-radial NSPC marker SOX2 (Figure 3C). Furthermore, the majority of radial processes positive for the radial NSPC marker Nestin were also GFP positive (83.7% ± 6.2%; Figure 3C). Cpt1a was virtually absent in doublecortin (DCX)-expressing neuronal progeny of hippocampal NSPCs (Figure 3D). Furthermore, Spot14 was co-expressed in Cpt1a-GFP-positive cells (Figures S3D and S3E), suggesting that FAO is indeed high in NSPCs and becomes downregulated with neuronal differentiation.

Cpt1a Is Required for Proper Neurogenesis In Vivo

To directly test for a role of Cpt1a-dependent FAO for NSPCs in vivo, we conditionally deleted Cpt1a specifically in adult quiescent NSPCs by crossing Cpt1a flox/flox mice (Cpt1a-conditional knockout [cKO]) (Schoors et al., 2015) with mice harboring tamoxifen (TAM)-inducible Spot14-driven Cre recombinase (S14iCre) (Knobloch et al., 2013) and yellow fluorescent protein

(YFP) reporter alleles in the ROSA locus (R26YFP), inducing recombination at seven weeks of age. The low recombination efficiency of the S14iCre mouse line resulted in sparse labeling of cells, allowing the identification and classification of labeled progeny into potential clones according to their spatial clustering, similarly to previously published analyses referred to as clonal analysis (Bonaguidi et al., 2011). However, it needs to be noted that the classification of cellular clusters into clones according to spatial distance only assumes common lineage and does not ultimately prove the presence of cells of clonal origin as this would require an additional level of genetic lineage tracing (e.g., through genetic bookmarking as previously used in NSPCs; Fuentealba et al., 2015).

We first analyzed cell cluster size distribution 8 days after the first TAM administration using the sparse labeling method and found that size and composition of cellular clusters was not significantly altered between control and Cpt1a-cKO mice, although no larger clones were found in Cpt1a-cKO (Figures S4A and S4D). At this time point, slightly lower numbers of clusters were found in Cpt1a-cKO mice compared to control mice (17 clones in 5 mice versus 24 clones in 4 mice), but the number of YFP-positive cells per mouse was not significantly lower in the Cpt1a-cKO mice compared to control mice (7.2 ± 4.5 versus 11 ± 3.7; $p > 0.1$). Detailed cluster analysis did not reveal significant changes (Figures S4B, S4C, and S4F), although a small decrease in clones containing only R and a small, non-significant increase in active clones in Cpt1a-cKO might be suggestive of an initial activation upon Cpt1a-dependent knockout of FAO.

Next, we analyzed cell cluster composition and number 25 days after the first TAM administration. These analyses revealed a dramatic decrease in the number of YFP-positive cells per clone in Cpt1a-cKO mice compared to control littermates (Figures 4A, 4B, and S4E). The majority of clones in the Cpt1a-cKO mice contained only one to two cells, whereas more than half of the clones in control mice were composed of three to 12 or even more cells (Figures 4A, 4B, and S4E), suggesting a massive impairment of NSPC expansion upon FAO knockout. Furthermore, fewer clones were found in Cpt1a-cKO mice compared to control mice (34 clones in seven Cpt1a-cKO mice versus 62 clones in three control mice), and the number of YFP-positive cells per mouse was significantly lower in the Cpt1a-cKO mice compared to control mice (Cpt1a-cKO: 12.8 ± 5.8 versus 111 ± 65.6 in control mice; $p < 0.05$), implying that FAO knockout leads to cell death. This was also reflected by a decrease in the number of radial-glia like NSPCs in Cpt1a-cKO compared to controls (Cpt1a-cKO: 2.6 ± 1.5 versus 17 ± 10.4 in control mice; $p = 0.06$).

A detailed analysis of the clone compositions revealed an increase in clones containing only one radial glia-like cell (R), a reduction in clones containing an R and neural progeny (N), an absence of clones containing a R, N and astrocytes (A), and an increase in clones without a R in Cpt1a-cKO mice compared to controls. Further, there was a strong reduction in the number of active clones (containing a radial glia-like cell that generated progeny) (Figures 4C–4D). Thus, genetic inhibition of FAO in adult hippocampal NSPCs results in fewer recombined cells indicative of cell death and smaller as well as less active clones indicative of reduced cell proliferation, thus corroborating the in vitro results upon FAO inhibition. However, the detailed impact of FAO on the specific cellular stage (quiescence, proliferation, cell death, and survival) cannot be answered unambiguously with these snapshot data. Given that FAO is used by both proliferating and quiescent NSPCs in vitro (although the latter have much higher FAO levels and depend more on it), it is indeed likely that the strong decrease in progeny generation upon FAO ablation is due to an influence of FAO on several cellular stages.

Small hairpin RNA (shRNA)-mediated knockdown of Cpt1a using in utero electroporation in the developing mouse cortex at mid-neurogenesis (embryonic day 13 [E13]) corroborated the importance of FAO for proper neurogenesis in vivo that has been also previously shown by Xie et al. (2016) (Figures S4I and S4J). Although NSPCs are more proliferative at this stage compared to adulthood (Farkas and Huttner, 2008), staining against endogenous Cpt1a confirmed that Cpt1a is also highly enriched in NSPCs lining the ventricle during development (Figure S4H). 24 hours after electroporation (corresponding to E14) (Figure S4J), proliferation at the apical surface was significantly reduced upon Cpt1a knockdown, and general disorganization of mitoses in the ventricular zone was observed (Figures S4K and S4L). Furthermore, we found a massive increase in cell death upon Cpt1a knockdown, as measured by the apoptotic marker cleaved caspase-3 (Figure S4M), corroborating the in vitro results.

Malonyl-CoA Levels Regulate NSPC Proliferation

Given the important role of FAO for NSPCs in vitro and in vivo, determined by fully blocking this pathway with genetic and pharmacological means, we next aimed to test the significance of this regulatory pathway for NSPC activity in a more physiological manner. Metabolic pathways are finely tunable through substrate availability and intrinsic levels of metabolites have been shown to determine pathway activity. Such shifts in pathway activity are likely to reflect better the actual physiological situation than switching off a pathway by genetic deletion of its key players. For FAO, the metabolite malonyl-CoA functions as the endogenous inhibitor of Cpt1a and serves at the same time as a substrate for de novo lipogenesis, thus it has also been termed a ''rheostat'' regulating these two lipid metabolic pathways (Foster, 2012; McGarry and Brown, 1997). Thus, we reasoned that elevating levels of malonyl-CoA decreases Cpt1a-dependent FAO in a physiological way rather than completely blocking it and provides sufficient substrate to fuel FASN-dependent de novo lipogenesis that is required for NSPC proliferation (Knobloch et al., 2013). However, it is not known if malonyl-CoA can be taken up by cells when provided extracellularly. Thus, we first tested if exogenously provided malonyl-CoA can be metabolized and detected intracellularly. We isolated lipids of proliferating, highly lipogenic NSPCs (Knobloch et al., 2013) that were incubated with radioactively labeled malonyl-CoA (^{14}C-malonyl-CoA) for 48 hr (Figure S5A). We detected incorporation of ^{14}C-malonyl-CoA in polar lipids and triacylglycerides (TAGs, neutral lipids) (Figure S5B), clearly showing that exogenous malonyl-CoA can indeed be utilized by NSPCs. Next, we tested if exogenously applied malonyl-CoA could prevent BMP4-mediated induction of NSPC quiescence. Adult NSPCs were exposed to

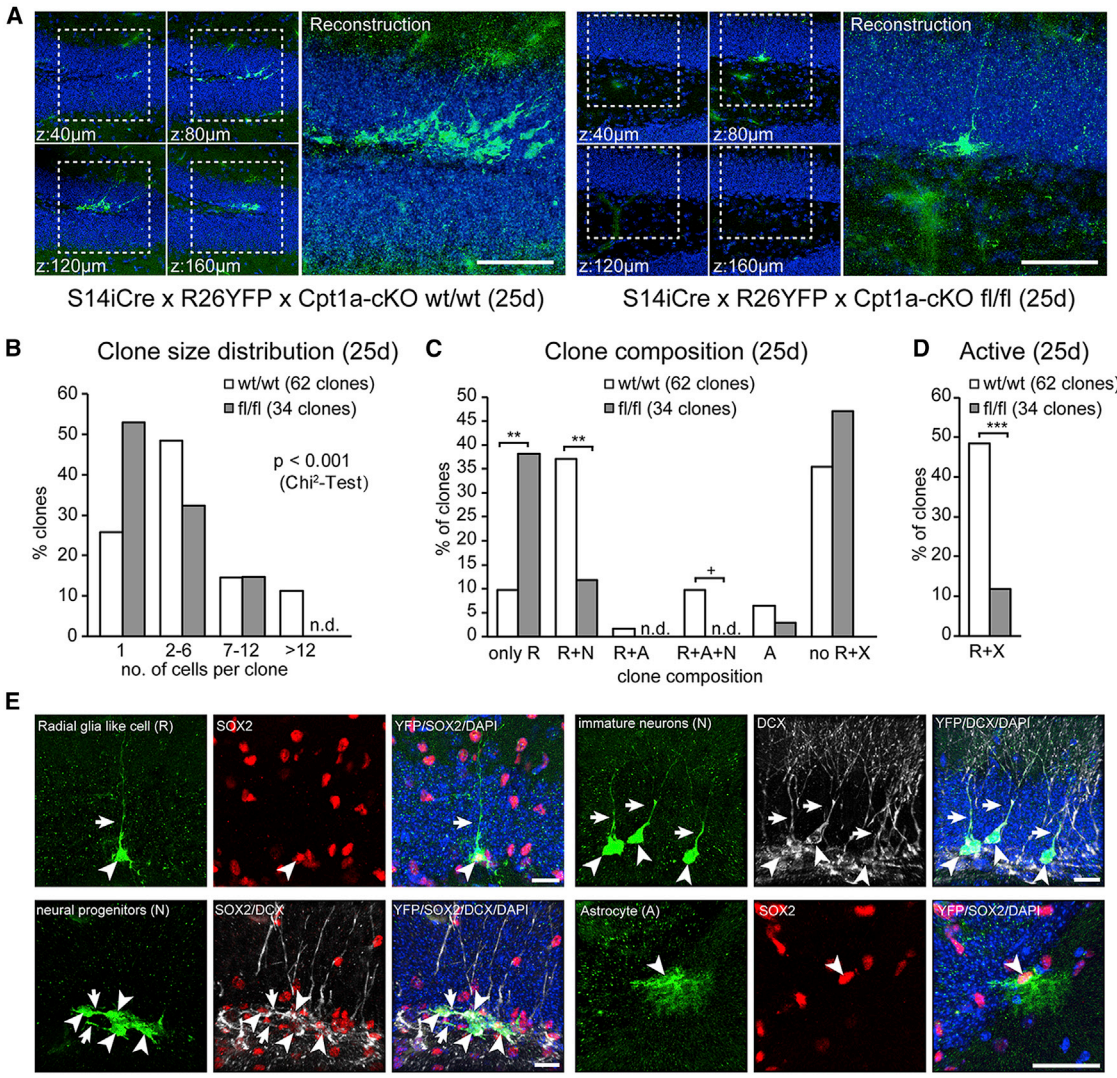

Figure 4. Cpt1a Is Required for Proper Neurogenesis In Vivo

(A) Conditional Cpt1a knockout in adult quiescent NSPCs, by crossing Cpt1a flox/flox mice with Spot14-driven CreER^{T2} recombinase mice and ROSA YFP reporter mice, leads to disturbed neurogenesis. Shown are representative confocal images (maximum projection) and a composite image showing the reconstruction of individual clones from Cpt1a-cKO wild-type (WT)/WT mice (left) and Cpt1a-cKO flox/flox mice (right) 25 days after first TAM induction. The boxed area is enlarged in the reconstruction panel.

(B) Clonal analysis reveals marked reduction in clone size in the Cpt1a-cKO flox/flox mice compared to Cpt1a-cKO WT/WT littermates.

(C) Detailed clone composition analysis shows a marked increase in clones containing only one radial glia-like cell (R), a great reduction in clones containing an R and neural progeny (N), absence of clones containing an R, N, and astrocytes (A) and a slight increase in clones without an R in Cpt1a-cKO flox/flox compared to Cpt1a-cKO WT/WT.

(D) Active clones containing a radial glia-like cell (R) and any kind of progeny (X) are strongly reduced in Cpt1a-cKO flox/flox, suggesting that FAO is required to allow proper neurogenesis.

(E) Representative confocal images of different types of recombined, YFP-positive cells from Cpt1a cKO WT/WT mice 25 days after the first TAM injection. Radial glia-like cells (R) have a triangular-shaped soma (arrowhead) in the subgranular zone (SGZ) with a radial, arborized process into GCL (arrow) and are SOX2 positive. Neural progenitors (N) are non-radial cells with their soma in the SGZ (arrowhead), with one or more horizontal processes (arrows), sometimes still SOX2, some already DCX positive. Immature neurons (N) have a round soma (arrowheads) in the granular cell layer (GCL) with a long vertical process (arrow), and are usually DCX positive. Astrocytes (A) are multi-process-containing, star-shaped or bushy cells in the SGZ/Hilus or GCL.

Scale bars represent 50 µm (A) and 40 µm (E). nd, not detected. ***$p < 0.001$; **$p < 0.01$, $^{+}p = 0.086$.

See also Figure S4.

BMP4-containing medium in the presence of different concentrations of malonyl-CoA (Figure 5A). Indeed, elevated levels of malonyl-CoA dose-dependently prevented the induction of quiescence, as measured using the cell cycle markers Ki67 and phosphorylated histone H3 (pH3) (Figure 5B). These data show that manipulating FAO through malonyl-CoA levels is

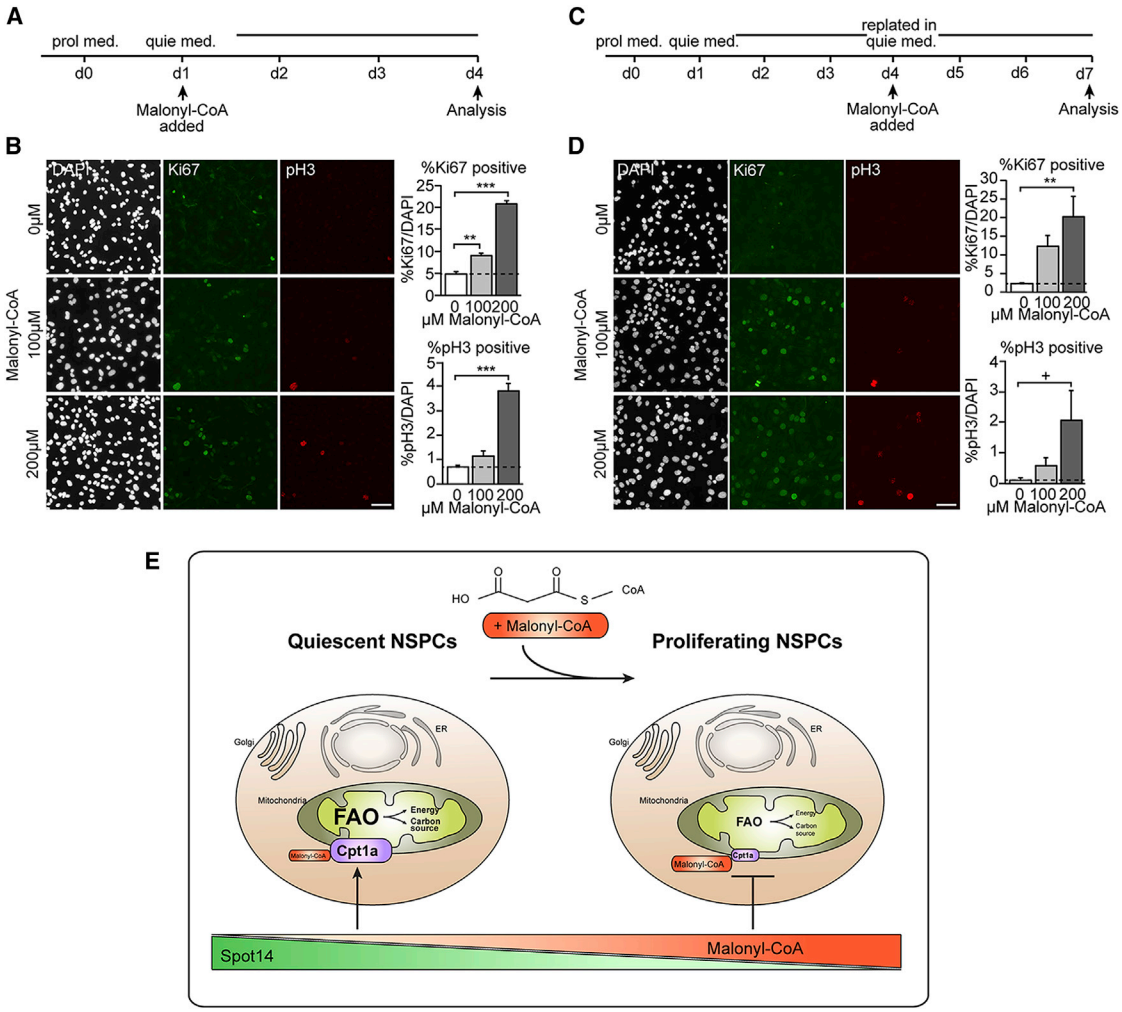

Figure 5. Malonyl-CoA Levels Regulate NSPC Proliferation

(A–E) Manipulating the levels of the physiological, intrinsic Cpt1a inhibitor malonyl-CoA is sufficient to prevent NSPC quiescence and to induce proliferation under quiescence conditions.

(A) Schematic outline of the experimental setup.

(B) Addition of malonyl-CoA (100 or 200 μM) at the beginning of quiescence induction is sufficient to prevent quiescence entry in a dose-dependent manner, as revealed with the cell cycle marker Ki67 and the mitotic marker phospho Histone 3 (pH3). Shown are representative images of indicated doses and the quantification of cycling and proliferating cells after 3 days of quiescence induction (mean ± SEM).

(C) Schematic outline of the experimental setup.

(D) Replating NSPCs after fully established quiescence in quiescence medium containing malonyl-CoA (100 or 200 μM) is sufficient to trigger cell cycle re-entry. This suggests that malonyl-CoA levels can overrule the present quiescence cues. Shown are representative images of indicated doses and the quantification of cycling and proliferating cells after three days of quiescence induction (mean ± SEM).

(E) Summary scheme of the described findings.

Scale bars represent 50 μm. ***$p < 0.001$; **$p < 0.01$, $^{+}p = 0.06$.

See also Figure S5.

sufficient to override BMP4-induced quiescence and keeps NSPCs in a proliferating state.

Next, we induced BMP4-mediated quiescence over 3 days, after which proliferation is almost completely inhibited, followed by replating the cells in quiescence medium together with malonyl-CoA (Figure 5C). Strikingly, we found that malonyl-CoA triggered NSPCs to enter the cell cycle in a dose-dependent manner, despite a fully established quiescence state and the continuous presence of quiescence cues (Figure 5D). This increased proliferation is most likely mediated by an increase in FASN-dependent de novo lipogenesis, as the addition of the FASN inhibitor Orlistat (Kridel et al., 2004) into the BMP4-containing quiescence medium significantly reduced remaining proliferation and abolished the pro-proliferative effect of malonyl-CoA when applied together with malonyl-CoA (Figures S5C and S5D). These data reveal that differential metabolic states are not a mere consequence of a given stem cell state but that manipulating levels of FAO through

malonyl-CoA is instructive to regulate the behavior of adult NSPCs (Figure 5E).

DISCUSSION

Due to its significance for brain function, understanding the mechanisms regulating adult hippocampal neurogenesis is important to advance the current knowledge of brain plasticity in health and disease (Jessberger and Gage, 2014). In addition to candidate-based approaches testing the role of well-studied signaling pathways that had been implicated in regulating embryonic neurogenesis such as Notch- and WNT-signaling, a series of recent studies used unbiased approaches to characterize gene expression profiles during distinct developmental stages in the course of adult neurogenesis (Bracko et al., 2012; Llorens-Bobadilla et al., 2015; Shin et al., 2015). These studies all pointed toward an important role of cellular metabolism and, more specifically, lipid metabolism in the regulation of the neurogenic process in the adult brain. Supporting this, we have previously shown that NSPCs in the adult brain depend on FASN-dependent de novo lipogenesis for proper proliferation and have identified Spot14, which is selectively expressed in largely quiescent NSPCs, as the brake on de novo lipogenesis (Knobloch et al., 2013, 2014). However, it remained unclear if Spot14 merely suppresses de novo lipogenesis to keep NSPCs in a quiescence state or if NSPC quiescence requires a specialized metabolic state.

We here used several complementary approaches in vitro and in vivo to show that quiescent NSPCs rely on FAO and that blocking this pathway pharmacologically or genetically leads to massive disturbance of NSPC behavior. Using in vitro approaches, we find clear evidence that inhibition of FAO leads to enhanced cell death of quiescent cells but also reduced proliferation. The conditional deletion of the rate-limiting enzyme Cpt1a in vivo also results in fewer and smaller cellular clusters, suggesting that the role for FAO in vivo resembles the described function of cultured NSPCs in vitro. The conditional deletion of Cpt1a in quiescent Spot14-positive NSPCs using the Spot14-CreER^{T2} mouse line allowed us to study the role of FAO on a specific NSPC population, reducing possible side effects of altering FAO in astrocytes, as would be the case by using other Cre-lines, such as GLAST-CreER^{T2} or Nestin-CreER^{T2} (Lagace et al., 2007; Mori et al., 2006). However, the low recombination efficiency of the Spot14-CreER^{T2}-line results in sparse labeling, enabling clonal analysis, but making assessments of proliferation or cell death with classical markers almost impossible. Thus, the detailed cellular effects (i.e., on exactly which stage FAO deletion exerts its main phenotype) remain to be elucidated and will require novel approaches to study neurogenesis within the endogenous niche such as chronic imaging.

Although glucose and lactate remain the main fuel sources for the brain (Lundgaard et al., 2015; Wyss et al., 2011), our data suggest that NSPCs might not only rely on these fuels. We provide mechanistic evidence that oxidized fatty acids are required for energy production and might serve as an alternative carbon source. Thus, our data reveal a metabolic shift in adult hippocampal NSPCs that defines the change from a quiescent to a proliferative state. Interestingly, many metabolic pathways are not only transcriptionally regulated but also highly dependent on substrate availability and inhibitory feedback loops of metabolic intermediates, providing a regulatory system than can be finely tuned rather than an "on-off" system (Lunt and Vander Heiden, 2011; Metallo and Vander Heiden, 2013). This is also the case for the breakdown and buildup of lipids (Houten et al., 2016; Menendez and Lupu, 2007). A central role in regulating the shift from FAO to lipogenesis appears to be mediated by the levels of malonyl-CoA. This physiological metabolite has been suggested to be a rheostat of stem cell fate (Folmes et al., 2013), being both an inhibitor of Cpt1a and a substrate for de novo lipogenesis (McGarry et al., 1983; Menendez and Lupu, 2007). Strikingly, we have previously shown that Spot14, which is highly expressed in quiescent NSPCs, indirectly reduces the levels of available malonyl-CoA and reduces lipid synthesis (Knobloch et al., 2013). BMP4-induced quiescent NSPCs recapitulate these features and show highly increased Spot14 levels and reduced malonyl-CoA levels, providing optimal conditions for FAO. Thus, our data support the hypothesis that malonyl-CoA acts as a rheostat with Spot14 taking a key role in this regulatory process (summarized in the graphical abstract). Our data corroborate previous findings by Stoll and colleagues who characterized the metabolic state of NSPCs in the subventricular zone (SVZ) and found that NSPCs in the adult SVZ depend on FAO for their proliferation as shown by infusing Etomoxir (thus pharmacologically inhibiting FAO) into the adult brain (Stoll et al., 2015). Interestingly, recent studies described a role for FAO in other stem cell systems: hematopoietic stem cells (HSCs) seem to require FAO to maintain their stem cell potential through a PPAR-delta mediated pathway and inhibition of FAO leads to HSC exhaustion (Ito et al., 2012). Similarly, quiescent muscle satellite cells are relying on FAO and pyruvate oxidation and undergo a metabolic shift toward glycolysis once they become activated (Ryall et al., 2015). Furthermore, a recent study has addressed the consequences of systemic inborn errors of FAO on brain development and showed that defects in FAO lead to enhanced progenitor generation and subsequently to a reduced embryonic NSPC pool (Xie et al., 2016). These studies emphasize the importance of FAO for proper stem cell behavior and suggest shared regulatory pathways involving FAO between different somatic stem cell types. Whether malonyl-CoA levels and Spot14 are the regulating entities in other somatic stem cells remains to be elucidated.

Excitingly, our data show that metabolic changes in the course of NSPC activation are not mere bystanders of other signaling pathways or transcriptional programs, but are effective to change NSPC behavior in vitro. Manipulating FAO through changing the levels of a single metabolite, its endogenous inhibitor malonyl-CoA, is sufficient to instruct quiescent NSPCs to enter cell cycle and to proliferate in vitro. Due to the short half-life of malonyl-CoA at 37°C (72 hr), in vivo experiments are currently not feasible. In contrast to the detrimental effects seen when completely switching off FAO genetically or pharmacologically, alteration of endogenous metabolite levels might better reflect the physiological relevance of metabolic shifts. Given the instructive role of metabolism on NSPC quiescence

and proliferation behavior, manipulations of the metabolic state may thus represent a novel approach to achieve enhanced neurogenesis in the aging brain or in disease states where NSPC activity is reduced.

EXPERIMENTAL PROCEDURES

Further details and an outline of the resources used in this work can be found in the Supplemental Experimental Procedures.

Mouse strains used were Cpt1a-EGFP reporter mice (STOCK Tg(Cpt1a-EGFP)IP41Gsat/Mmucd, MMRRC), Cpt1a cKO mice (Schoors et al., 2015), Spot14CreERT2 mice (S14iCre) Knobloch et al., 2013), ROSA26 YFP reporter mice (R26YFP), and C57/Bl6 mice (Janvier). All animal experiments were performed according to Swiss regulatory standards and approved by the Veterinary office of the Canton of Zurich. Cre-mediated recombination was induced by intraperitoneal injections of tamoxifen (180 mg/kg) at the age of 6 to 7 weeks. Lentiviral constructs were designed and viruses produced as previously described (Knobloch et al., 2013). Adult mouse DG NSPCs were cultured in DMEM with Ham's F12, supplemented with N2 supplement plus epidermal growth factor (EGF), fibroblast growth factor, and heparin (Knobloch et al., 2013; Ray and Gage, 2006). Quiescence was induced over three days replacing EGF with BMP4, as previously described (Martynoga et al., 2013; Mira et al., 2010). For Cpt1a inhibition, Etomoxir or malonyl-CoA was added to the medium as outlined in the figures. Proteomic analysis was done according to previously established protocols (Wiśniewski et al., 2009). Radioactive FAO measurements were done using labeled ^{3}H-palmitic acid and ^{14}C-palmitic acid, and the amount of tritiated water or $^{14}CO_2$ generated was assessed (Djouadi et al., 2003; Huynh et al., 2014). Quiescent and proliferating NSPCs were collected for RNA and protein isolation, and established protocols were used for subsequent processing and analysis (Knobloch et al., 2013). In utero electroporation of Cpt1a and control shRNA plasmid DNA into mouse embryos (embryonic day 13 [E13]) was carried out as described previously (Asami et al., 2011). For immunohistochemical analyses, brain tissues were sectioned, stained, and imaged using previously published methods (Bonaguidi et al., 2011; Knobloch et al., 2013). Mass spectrometry measurements to assess the amount of malonyl-CoA and to determine the energy charge were done with cellular extracts using liquid chromatography-tandem mass spectrometry LC-MS/MS (Knobloch et al., 2013; Schoors et al., 2015). To analyze C13 incorporation, quiescent and proliferating NSPCs were incubated 24 hr prior to collection/extraction with ^{13}C-palmitic acid and analyzed with gas chromatography-mass spectrometry (GC-MS) as previously described (Schoors et al., 2015). Statistical analysis was performed using unpaired t tests, paired t tests, and one-way-ANOVA or two-way-ANOVA, followed by Holm-Sidak's multiple comparisons tests. Significance levels are set at $p < 0.05$.

SUPPLEMENTAL INFORMATION

Supplemental Information includes Supplemental Experimental Procedures, five figures, and three tables and can be found with this article online at http://dx.doi.org/10.1016/j.celrep.2017.08.029.

AUTHOR CONTRIBUTIONS

M.K. co-developed the concept, performed the experiments, analyzed the data, and co-wrote the paper. G.-A.P. and M.K. performed the experiments in the embryonic brain. B.G. and M.K. performed the metabolite tracing experiments. T.W. performed the proteomics experiments. W.J.K. and M.K. performed the radioactive tracing experiments and the gene expression analyses. M.K. performed the in vivo experiments, with help from G.-A.P and D.L.M. D.L.M. contributed to in vivo Cpt1a expression analysis. M.H. and N.Z. performed malonyl-CoA measurements. P.C. contributed reagents and transgenic mice and provided critical conceptual input. All authors revised the manuscript. S.J. developed the concept and wrote the paper. The authors declare that patent applications concerning this work are pending.

ACKNOWLEDGMENTS

We thank D.C. Lie for comments on the manuscript and the ZMB (UZH) and BIOP (EPFL) imaging facilities for help with imaging. We also thank J. Grossmann, P. Gehrig, and B. Roschitzki of the FGCZ (UZH and ETHZ) and the Zurich Neuroscience Center (ZNZ) of UZH and ETHZ. This study was supported by the Swiss National Science Foundation (BSCGI0_157859; 31003A_156943), the EMBO Young Investigator Program, the Théodore Ott Foundation, the Novartis Foundation, and the European Research Council (to S.J.). M.K. was supported by the Janggen-Pöhn Foundation, G.A.P. by an EMBO long-term fellowship, D.L.M. by a Human Frontier Science Program long-term fellowship, and T.W. by the Boehringer Ingelheim Fonds.

Received: July 14, 2017
Revised: July 27, 2017
Accepted: August 6, 2017
Published: August 29, 2017

REFERENCES

Ables, J.L., Decarolis, N.A., Johnson, M.A., Rivera, P.D., Gao, Z., Cooper, D.C., Radtke, F., Hsieh, J., and Eisch, A.J. (2010). Notch1 is required for maintenance of the reservoir of adult hippocampal stem cells. J. Neurosci. *30*, 10484–10492.

Asami, M., Pilz, G.A., Ninkovic, J., Godinho, L., Schroeder, T., Huttner, W.B., and Götz, M. (2011). The role of Pax6 in regulating the orientation and mode of cell division of progenitors in the mouse cerebral cortex. Development *138*, 5067–5078.

Bonaguidi, M.A., Wheeler, M.A., Shapiro, J.S., Stadel, R.P., Sun, G.J., Ming, G.L., and Song, H. (2011). In vivo clonal analysis reveals self-renewing and multipotent adult neural stem cell characteristics. Cell *145*, 1142–1155.

Bracko, O., Singer, T., Aigner, S., Knobloch, M., Winner, B., Ray, J., Clemenson, G.D., Jr., Suh, H., Couillard-Despres, S., Aigner, L., et al. (2012). Gene expression profiling of neural stem cells and their neuronal progeny reveals IGF2 as a regulator of adult hippocampal neurogenesis. J. Neurosci. *32*, 3376–3387.

Chorna, N.E., Santos-Soto, I.J., Carballeira, N.M., Morales, J.L., de la Nuez, J., Cátala-Valentin, A., Chornyy, A.P., Vázquez-Montes, A., and De Ortiz, S.P. (2013). Fatty acid synthase as a factor required for exercise-induced cognitive enhancement and dentate gyrus cellular proliferation. PLoS ONE *8*, e77845.

Christian, K.M., Song, H., and Ming, G.L. (2014). Functions and dysfunctions of adult hippocampal neurogenesis. Annu. Rev. Neurosci. *37*, 243–262.

Clelland, C.D., Choi, M., Romberg, C., Clemenson, G.D., Jr., Fragniere, A., Tyers, P., Jessberger, S., Saksida, L.M., Barker, R.A., Gage, F.H., et al. (2009). A functional role for adult hippocampal neurogenesis in spatial pattern separation. Science *325*, 210–213.

Colbert, C.L., Kim, C.W., Moon, Y.A., Henry, L., Palnitkar, M., McKean, W.B., Fitzgerald, K., Deisenhofer, J., Horton, J.D., and Kwon, H.J. (2010). Crystal structure of Spot 14, a modulator of fatty acid synthesis. Proc. Natl. Acad. Sci. USA *107*, 18820–18825.

David, R. (2011). Stem cells: LKB1 maintains the balance. Nat. Rev. Mol. Cell Biol. *12*, 4.

Deng, W., Aimone, J.B., and Gage, F.H. (2010). New neurons and new memories: how does adult hippocampal neurogenesis affect learning and memory? Nat. Rev. Neurosci. *11*, 339–350.

Djouadi, F., Bonnefont, J.P., Munnich, A., and Bastin, J. (2003). Characterization of fatty acid oxidation in human muscle mitochondria and myoblasts. Mol. Genet. Metab. *78*, 112–118.

Dupret, D., Revest, J.M., Koehl, M., Ichas, F., De Giorgi, F., Costet, P., Abrous, D.N., and Piazza, P.V. (2008). Spatial relational memory requires hippocampal adult neurogenesis. PLoS ONE *3*, e1959.

Ehm, O., Göritz, C., Covic, M., Schäffner, I., Schwarz, T.J., Karaca, E., Kempkes, B., Kremmer, E., Pfrieger, F.W., Espinosa, L., et al. (2010).

RBPJkappa-dependent signaling is essential for long-term maintenance of neural stem cells in the adult hippocampus. J. Neurosci. *30*, 13794–13807.

Espósito, M.S., Piatti, V.C., Laplagne, D.A., Morgenstern, N.A., Ferrari, C.C., Pitossi, F.J., and Schinder, A.F. (2005). Neuronal differentiation in the adult hippocampus recapitulates embryonic development. J. Neurosci. *25*, 10074–10086.

Farkas, L.M., and Huttner, W.B. (2008). The cell biology of neural stem and progenitor cells and its significance for their proliferation versus differentiation during mammalian brain development. Curr. Opin. Cell Biol. *20*, 707–715.

Folmes, C.D., Nelson, T.J., Martinez-Fernandez, A., Arrell, D.K., Lindor, J.Z., Dzeja, P.P., Ikeda, Y., Perez-Terzic, C., and Terzic, A. (2011). Somatic oxidative bioenergetics transitions into pluripotency-dependent glycolysis to facilitate nuclear reprogramming. Cell Metab. *14*, 264–271.

Folmes, C.D., Park, S., and Terzic, A. (2013). Lipid metabolism greases the stem cell engine. Cell Metab. *17*, 153–155.

Foster, D.W. (2012). Malonyl-CoA: the regulator of fatty acid synthesis and oxidation. J. Clin. Invest. *122*, 1958–1959.

Fuentealba, L.C., Rompani, S.B., Parraguez, J.I., Obernier, K., Romero, R., Cepko, C.L., and Alvarez-Buylla, A. (2015). Embryonic origin of postnatal neural stem cells. Cell *161*, 1644–1655.

Ge, S., Yang, C.H., Hsu, K.S., Ming, G.L., and Song, H. (2007). A critical period for enhanced synaptic plasticity in newly generated neurons of the adult brain. Neuron *54*, 559–566.

Gonçalves, J.T., Schafer, S.T., and Gage, F.H. (2016). Adult neurogenesis in the hippocampus: from stem cells to behavior. Cell *167*, 897–914.

Gong, S., Zheng, C., Doughty, M.L., Losos, K., Didkovsky, N., Schambra, U.B., Nowak, N.J., Joyner, A., Leblanc, G., Hatten, M.E., and Heintz, N. (2003). A gene expression atlas of the central nervous system based on bacterial artificial chromosomes. Nature *425*, 917–925.

Homem, C.C., Repic, M., and Knoblich, J.A. (2015). Proliferation control in neural stem and progenitor cells. Nature reviews *16*, 647–659.

Houten, S.M., and Wanders, R.J. (2010). A general introduction to the biochemistry of mitochondrial fatty acid β-oxidation. J. Inherit. Metab. Dis. *33*, 469–477.

Houten, S.M., Violante, S., Ventura, F.V., and Wanders, R.J. (2016). The biochemistry and physiology of mitochondrial fatty acid β-oxidation and its genetic disorders. Annu. Rev. Physiol. *78*, 23–44.

Huynh, F.K., Green, M.F., Koves, T.R., and Hirschey, M.D. (2014). Measurement of fatty acid oxidation rates in animal tissues and cell lines. Methods Enzymol. *542*, 391–405.

Ito, K., and Suda, T. (2014). Metabolic requirements for the maintenance of self-renewing stem cells. Nat. Rev. Mol. Cell Biol. *15*, 243–256.

Ito, K., Carracedo, A., Weiss, D., Arai, F., Ala, U., Avigan, D.E., Schafer, Z.T., Evans, R.M., Suda, T., Lee, C.H., and Pandolfi, P.P. (2012). A PML–PPAR-δ pathway for fatty acid oxidation regulates hematopoietic stem cell maintenance. Nat. Med. *18*, 1350–1358.

Jessberger, S., and Gage, F.H. (2014). Adult neurogenesis: bridging the gap between mice and humans. Trends Cell Biol. *24*, 558–563.

Kempermann, G., Krebs, J., and Fabel, K. (2008). The contribution of failing adult hippocampal neurogenesis to psychiatric disorders. Curr. Opin. Psychiatry *21*, 290–295.

Knobloch, M., Braun, S.M., Zurkirchen, L., von Schoultz, C., Zamboni, N., Araúzo-Bravo, M.J., Kovacs, W.J., Karalay, O., Suter, U., Machado, R.A., et al. (2013). Metabolic control of adult neural stem cell activity by Fasn-dependent lipogenesis. Nature *493*, 226–230.

Knobloch, M., von Schoultz, C., Zurkirchen, L., Braun, S.M., Vidmar, M., and Jessberger, S. (2014). SPOT14-positive neural stem/progenitor cells in the hippocampus respond dynamically to neurogenic regulators. Stem Cell Reports *3*, 735–742.

Kridel, S.J., Axelrod, F., Rozenkrantz, N., and Smith, J.W. (2004). Orlistat is a novel inhibitor of fatty acid synthase with antitumor activity. Cancer Res. *64*, 2070–2075.

Lagace, D.C., Whitman, M.C., Noonan, M.A., Ables, J.L., DeCarolis, N.A., Arguello, A.A., Donovan, M.H., Fischer, S.J., Farnbauch, L.A., Beech, R.D., et al. (2007). Dynamic contribution of nestin-expressing stem cells to adult neurogenesis. J. Neurosci. *27*, 12623–12629.

Leone, T.C., Weinheimer, C.J., and Kelly, D.P. (1999). A critical role for the peroxisome proliferator-activated receptor alpha (PPARalpha) in the cellular fasting response: the PPARalpha-null mouse as a model of fatty acid oxidation disorders. Proc. Natl. Acad. Sci. USA *96*, 7473–7478.

Llorens-Bobadilla, E., Zhao, S., Baser, A., Saiz-Castro, G., Zwadlo, K., and Martin-Villalba, A. (2015). Single-cell transcriptomics reveals a population of dormant neural stem cells that become activated upon brain injury. Cell Stem Cell *17*, 329–340.

Lugert, S., Basak, O., Knuckles, P., Haussler, U., Fabel, K., Götz, M., Haas, C.A., Kempermann, G., Taylor, V., and Giachino, C. (2010). Quiescent and active hippocampal neural stem cells with distinct morphologies respond selectively to physiological and pathological stimuli and aging. Cell Stem Cell *6*, 445–456.

Lundgaard, I., Li, B., Xie, L., Kang, H., Sanggaard, S., Haswell, J.D., Sun, W., Goldman, S., Blekot, S., Nielsen, M., et al. (2015). Direct neuronal glucose uptake heralds activity-dependent increases in cerebral metabolism. Nat. Commun. *6*, 6807.

Lunt, S.Y., and Vander Heiden, M.G. (2011). Aerobic glycolysis: meeting the metabolic requirements of cell proliferation. Annu. Rev. Cell Dev. Biol. *27*, 441–464.

Martynoga, B., Mateo, J.L., Zhou, B., Andersen, J., Achimastou, A., Urbán, N., van den Berg, D., Georgopoulou, D., Hadjur, S., Wittbrodt, J., et al. (2013). Epigenomic enhancer annotation reveals a key role for NFIX in neural stem cell quiescence. Genes Dev. *27*, 1769–1786.

McGarry, J.D., and Brown, N.F. (1997). The mitochondrial carnitine palmitoyltransferase system. From concept to molecular analysis. Eur. J. Biochem. *244*, 1–14.

McGarry, J.D., Mills, S.E., Long, C.S., and Foster, D.W. (1983). Observations on the affinity for carnitine, and malonyl-CoA sensitivity, of carnitine palmitoyltransferase I in animal and human tissues. Demonstration of the presence of malonyl-CoA in non-hepatic tissues of the rat. Biochem. J. *214*, 21–28.

Menendez, J.A., and Lupu, R. (2007). Fatty acid synthase and the lipogenic phenotype in cancer pathogenesis. Nat. Rev. Cancer *7*, 763–777.

Mergenthaler, P., Lindauer, U., Dienel, G.A., and Meisel, A. (2013). Sugar for the brain: the role of glucose in physiological and pathological brain function. Trends Neurosci. *36*, 587–597.

Metallo, C.M., and Vander Heiden, M.G. (2013). Understanding metabolic regulation and its influence on cell physiology. Mol. Cell *49*, 388–398.

Ming, G.L., and Song, H. (2011). Adult neurogenesis in the mammalian brain: significant answers and significant questions. Neuron *70*, 687–702.

Mira, H., Andreu, Z., Suh, H., Lie, D.C., Jessberger, S., Consiglio, A., San Emeterio, J., Hortigüela, R., Marqués-Torrejón, M.A., Nakashima, K., et al. (2010). Signaling through BMPR-IA regulates quiescence and long-term activity of neural stem cells in the adult hippocampus. Cell Stem Cell *7*, 78–89.

Mori, T., Tanaka, K., Buffo, A., Wurst, W., Kühn, R., and Götz, M. (2006). Inducible gene deletion in astroglia and radial glia–a valuable tool for functional and lineage analysis. Glia *54*, 21–34.

Nakashiba, T., Cushman, J.D., Pelkey, K.A., Renaudineau, S., Buhl, D.L., McHugh, T.J., Rodriguez Barrera, V., Chittajallu, R., Iwamoto, K.S., McBain, C.J., et al. (2012). Young dentate granule cells mediate pattern separation, whereas old granule cells facilitate pattern completion. Cell *149*, 188–201.

Ray, J., and Gage, F.H. (2006). Differential properties of adult rat and mouse brain-derived neural stem/progenitor cells. Mol. Cell. Neurosci. *31*, 560–573.

Ryall, J.G., Dell'Orso, S., Derfoul, A., Juan, A., Zare, H., Feng, X., Clermont, D., Koulnis, M., Gutierrez-Cruz, G., Fulco, M., and Sartorelli, V. (2015). The NAD(+)-dependent SIRT1 deacetylase translates a metabolic switch into regulatory epigenetics in skeletal muscle stem cells. Cell Stem Cell *16*, 171–183.

Sahay, A., Scobie, K.N., Hill, A.S., O'Carroll, C.M., Kheirbek, M.A., Burghardt, N.S., Fenton, A.A., Dranovsky, A., and Hen, R. (2011a). Increasing adult

hippocampal neurogenesis is sufficient to improve pattern separation. Nature *472*, 466–470.

Sahay, A., Wilson, D.A., and Hen, R. (2011b). Pattern separation: a common function for new neurons in hippocampus and olfactory bulb. Neuron *70*, 582–588.

Scharfman, H.E., and Hen, R. (2007). Neuroscience. Is more neurogenesis always better? Science *315*, 336–338.

Schoors, S., Bruning, U., Missiaen, R., Queiroz, K.C., Borgers, G., Elia, I., Zecchin, A., Cantelmo, A.R., Christen, S., Goveia, J., et al. (2015). Fatty acid carbon is essential for dNTP synthesis in endothelial cells. Nature *520*, 192–197.

Seri, B., García-Verdugo, J.M., McEwen, B.S., and Alvarez-Buylla, A. (2001). Astrocytes give rise to new neurons in the adult mammalian hippocampus. J. Neurosci. *21*, 7153–7160.

Shin, J., Berg, D.A., Zhu, Y., Shin, J.Y., Song, J., Bonaguidi, M.A., Enikolopov, G., Nauen, D.W., Christian, K.M., Ming, G.L., and Song, H. (2015). Single-cell RNA-seq with waterfall reveals molecular cascades underlying adult neurogenesis. Cell Stem Cell *17*, 360–372.

Spalding, K.L., Bergmann, O., Alkass, K., Bernard, S., Salehpour, M., Huttner, H.B., Boström, E., Westerlund, I., Vial, C., Buchholz, B.A., et al. (2013). Dynamics of hippocampal neurogenesis in adult humans. Cell *153*, 1219–1227.

Stoll, E.A., Makin, R., Sweet, I.R., Trevelyan, A.J., Miwa, S., Horner, P.J., and Turnbull, D.M. (2015). Neural stem cells in the adult subventricular zone oxidize fatty acids to produce energy and support neurogenic activity. Stem Cells *33*, 2306–2319.

Toni, N., Laplagne, D.A., Zhao, C., Lombardi, G., Ribak, C.E., Gage, F.H., and Schinder, A.F. (2008). Neurons born in the adult dentate gyrus form functional synapses with target cells. Nat. Neurosci. *11*, 901–907.

van Praag, H., Schinder, A.F., Christie, B.R., Toni, N., Palmer, T.D., and Gage, F.H. (2002). Functional neurogenesis in the adult hippocampus. Nature *415*, 1030–1034.

Wiśniewski, J.R., Zougman, A., Nagaraj, N., and Mann, M. (2009). Universal sample preparation method for proteome analysis. Nat. Methods *6*, 359–362.

Wyss, M.T., Jolivet, R., Buck, A., Magistretti, P.J., and Weber, B. (2011). In vivo evidence for lactate as a neuronal energy source. J. Neurosci. *31*, 7477–7485.

Xie, Z., Jones, A., Deeney, J.T., Hur, S.K., and Bankaitis, V.A. (2016). Inborn errors of long-chain fatty acid β-oxidation link neural stem cell self-renewal to autism. Cell Rep. *14*, 991–999.

Zhao, C., Teng, E.M., Summers, R.G., Jr., Ming, G.L., and Gage, F.H. (2006). Distinct morphological stages of dentate granule neuron maturation in the adult mouse hippocampus. J. Neurosci. *26*, 3–11.

Cell Reports, Volume *20*

Supplemental Information

A Fatty Acid Oxidation-Dependent Metabolic Shift Regulates Adult Neural Stem Cell Activity

Marlen Knobloch, Gregor-Alexander Pilz, Bart Ghesquière, Werner J. Kovacs, Thomas Wegleiter, Darcie L. Moore, Martina Hruzova, Nicola Zamboni, Peter Carmeliet, and Sebastian Jessberger

SUPPLEMENTAL FIGURES

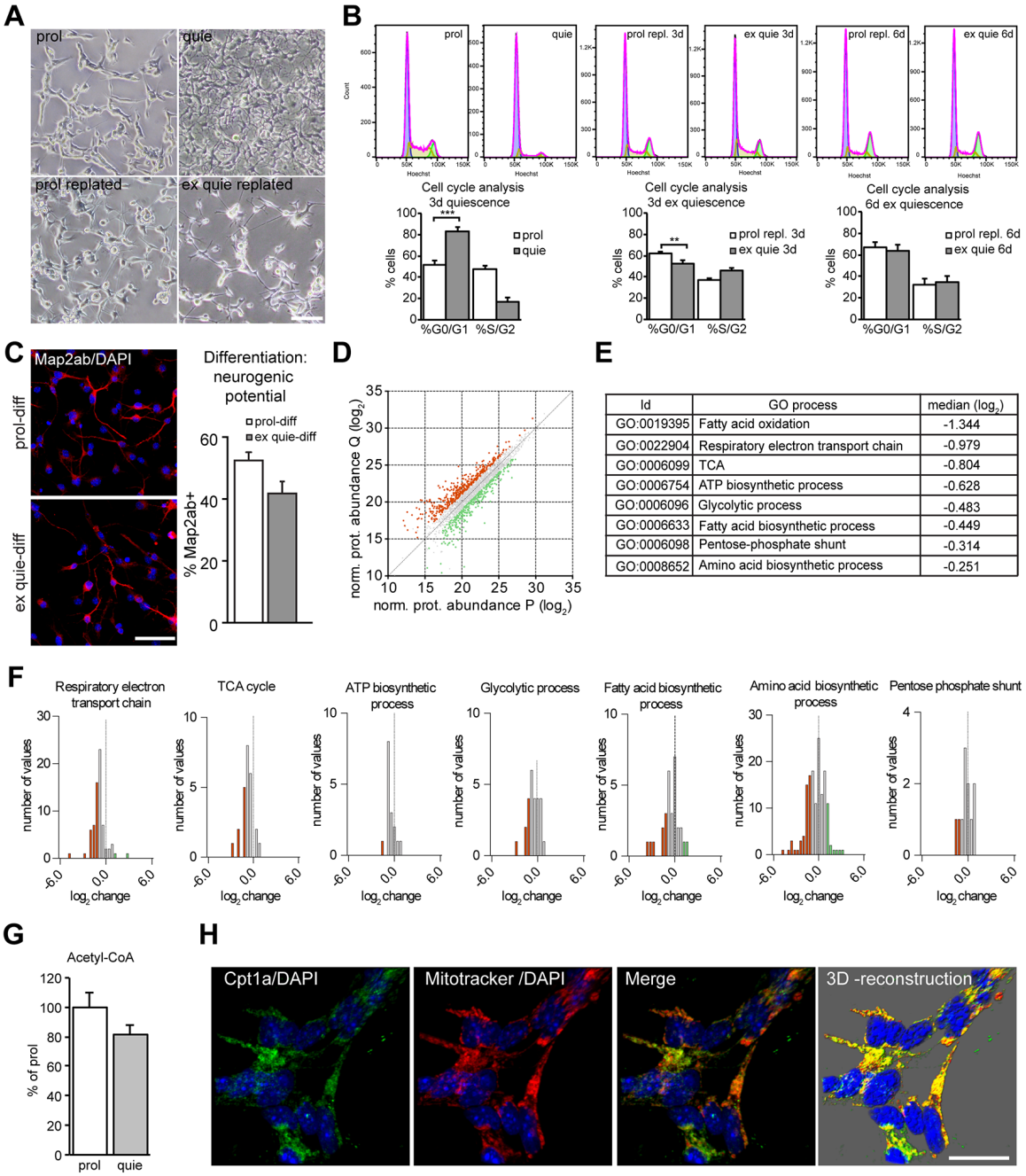

Id	GO process	median (log_2)
GO:0019395	Fatty acid oxidation	-1.344
GO:0022904	Respiratory electron transport chain	-0.979
GO:0006099	TCA	-0.804
GO:0006754	ATP biosynthetic process	-0.628
GO:0006096	Glycolytic process	-0.483
GO:0006633	Fatty acid biosynthetic process	-0.449
GO:0006098	Pentose-phosphate shunt	-0.314
GO:0008652	Amino acid biosynthetic process	-0.251

Figure S1 (related to Figure 1): Quiescent NSPCs have a high rate of fatty acid oxidation (FAO). A) Representative images of reversible BMP4-induced quiescence in NSPCs. Shown are NSPCs kept under proliferating conditions (prol), after 3 days of quiescence induction (quie), proliferating NSPCs that were

replated into proliferation medium (prol replated) and previously quiescent NSPCs that were replated into proliferation medium and kept for 3 days under proliferation conditions (ex quie replated). **B**) Flow cytometry histograms showing the DNA profile of proliferating (prol) and quiescent (quie) NSPCs and of previously quiescent NSCPs that have been replated into proliferation medium for 3 days (ex quie 3d) or 6 days (ex quie 6d). The corresponding proliferating control NSCPs were replated accordingly (prol repl. 3d and prol repl. 6d). Three days of quiescence treatment significantly decreases the amount of proliferating cells. Replating quiescent NSPCs into proliferation medium induces cell proliferation, showing the reversibility of this *in vitro* quiescence. Although 3 days re-exposure to proliferation medium led to a very similar proliferation profile as seen in NSPCs not exposed to quiescence, there were still significant differences, which were gone after 6 days of re-exposure to proliferation medium. Bars represent mean ± SEM. **C**) The neurogenic potential upon differentiation was not altered upon previous quiescence exposure, further demonstrating the reversibility of the system. Shown are representative images of NSPCs that were allowed to spontaneously differentiate for 9 days upon growth factor removal. Prior to differentiation, NSPCs were either exposed 3 days to quiescence cues followed by 3 days proliferation medium (ex quie-diff) or kept all the time under proliferation conditions (prol-diff). Map2ab marks neurons. Quantification represents mean ± SEM. **D**) Comparative analysis of the proteome of proliferating and quiescent NSPCs reveals proteins involved in FAO to be enriched in quiescent NSPCs. The dot plot shows proteins changed significantly

at least two fold ($\log_2 \geq |1|$) in quiescent (red) and proliferating (green) NSPCs. **E)** Shown is the median abundance of proteins belonging to the represented GO terms. Only the GO term “Fatty acid oxidation” was changed more than 2 fold (median higher than $\log_2 \geq |1|$). **F)** Histograms show the normalized abundance of proteins belonging to the indicated GO terms, detected in the mass spectrometric comparison of proliferating and quiescent NSPCs. (Gray = expression change of $\log_2 < |1|$, red = expression change of $\log_2 \leq -1$, enriched in quiescent NSPCs, green = expression change of $\log_2 \geq 1$, enriched in proliferating NSPCs). **G**) Acetyl-CoA does not differ significantly between quiescent and proliferating NSPCs, as measured by mass spectrometry (mean + SEM). **H**) Cpt1a in proliferating NSPCs co-localizes with the mitochondrial marker Mitotracker. Shown are representative confocal images of maximum projections of individual channels and a 3D-reconstruction.

Scale bar: 100μm (A), 50μm (C), 20μm (H); ***$p < 0.001$, **$p < 0.01$

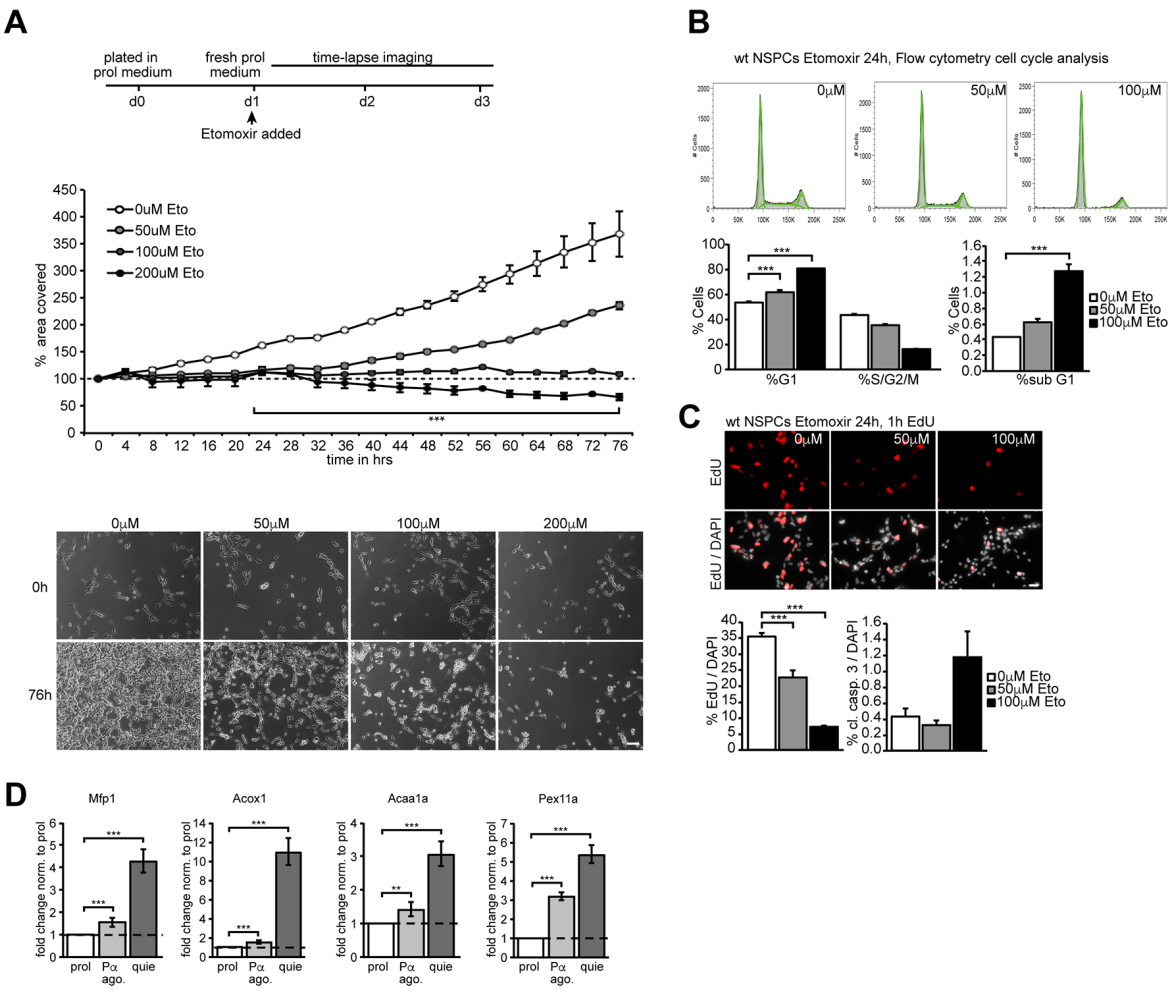

Figure S2 (related to Figure 2): Pharmacological blocking of FAO in proliferating NSPCs decreases proliferation. A) Time-lapse analysis of proliferating NSPCs exposed to various doses of the irreversible Cpt1 inhibitor Etomoxir (50, 100 and 200μM). Shown are a schematic outline of the experimental setup, the quantification of the area covered by proliferating NSPCs over time, and representative images. The quantification of the percent area covered by proliferating NSPCs reveals a significant decrease in proliferation for all doses tested. **B)** Flow cytometry-based cell cycle analysis confirms a decrease in proliferation with Etomoxir in proliferating NSPCs. Shown are

Histograms of DNA profiles after 24h of exposure with the indicated doses of Etomoxir (50 and 100μM) and the corresponding quantification (left bar graph). Right bars show the percentage of cells in Sub-G1 as a readout for cell death. 100μM Etomoxir lead to a mild but significant increase in cell death. **C**) The decrease in proliferation upon Etomoxir treatment is also apparent using an EdU-pulse to label cells in S-phase. With 50μM or 100μM Etomoxir for 24h, the amount of proliferating NSPCs decreased significantly, whereas the increase in cell death (cleaved caspase-3) was mild and non-significant. Shown are representative images of the different conditions and quantification of proliferation and cell death. **D**) Treatment with the PPARα agonist WY14643 led to an upregulation of PPARα target FAO genes in proliferating NSPCs compared to control NSPCs, however, to a far lesser extent than in quiescent NSPCs. Shown are the mRNA expression levels (mean fold change ± range) of multifunctional protein 1 (Mfp1), Acyl-CoA oxidase 1 (Acox1), peroxisomal 3-ketoacyl-CoA thiolase A (Acaa1a) and peroxisomal biogenesis factor 11 alpha (Pex11a).

Scale bars: 50μm; ***$p < 0.001$, **$p < 0.01$.

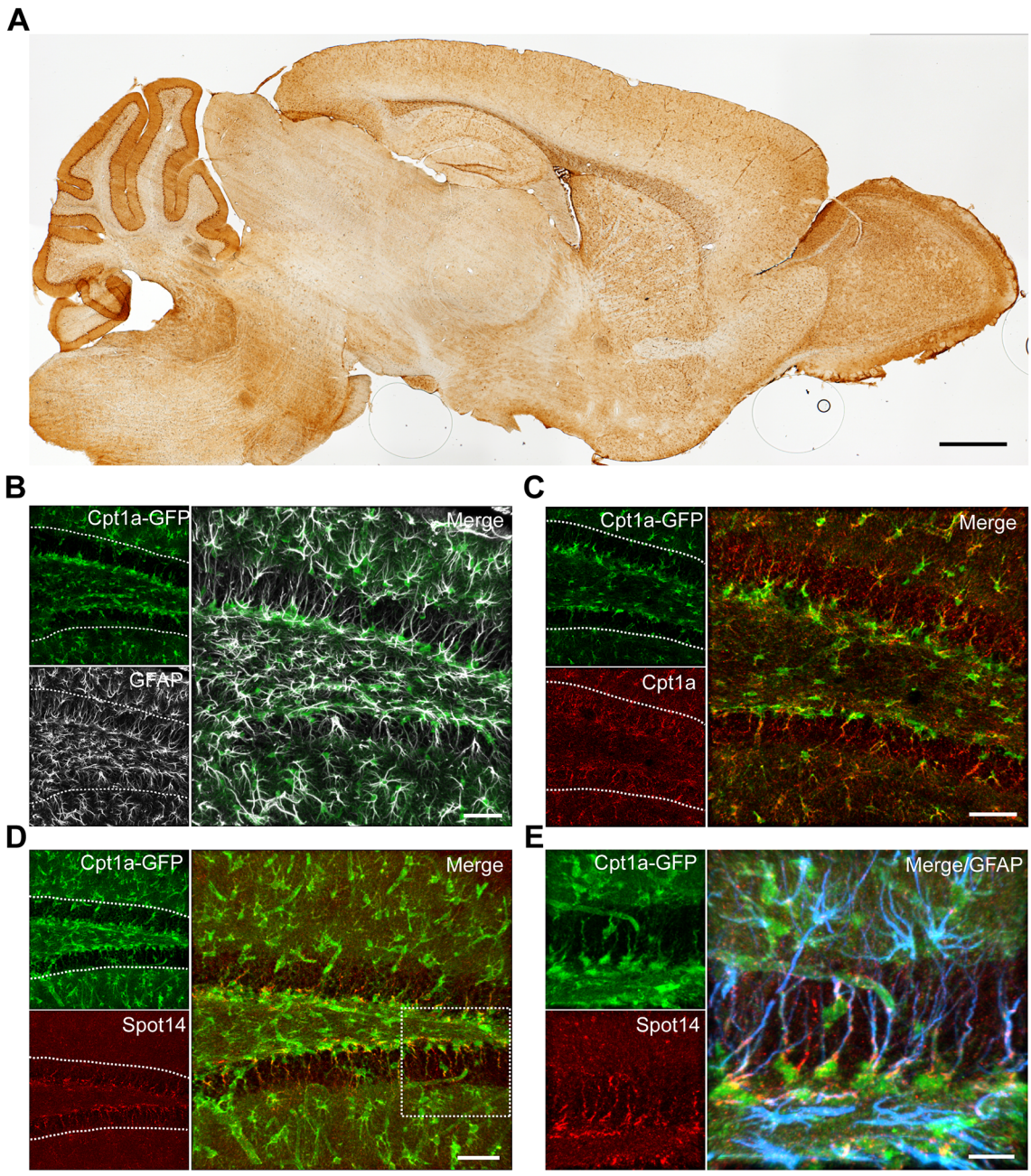

Figure S3 (related to Figure 3): Cpt1a is expressed in quiescent NSPCs *in vivo* and co-labels with the quiescence marker Spot14. A) DAB-staining against GFP on a sagittal section of a 2-month-old Cpt1a-GFP reporter mouse. **B**) Co-staining for Cpt1a-GFP and for glial fibrillary acidic protein (GFAP) shows

that GFP positive cells outside the subgranular zone of the DG are astrocytes. Shown is a representative confocal image (maximum projection) from a 2-month-old Cpt1a-GFP reporter mouse. Dotted lines show the outline of the granular zone of the DG. **C**) Co-staining for Cpt1a-GFP and endogenous Cpt1a protein shows that the Cpt1a-GFP reporter mouse faithfully reports Cpt1a expression. Shown is a representative confocal image (maximum projection) from a 2-month-old Cpt1a-GFP reporter mouse. Dotted lines show the outline of the granular zone of the DG. **D**) Co-staining for Cpt1a-GFP and endogenous Spot14 protein reveals that NSPCs expressing Spot14 are also positive for GFP. Shown is a representative confocal image (maximum projection) from a 2-month-old Cpt1a-GFP reporter mouse. Dotted lines show the outline of the granular zone of the DG. Note the increase in GFP signal due to harsh epitope retrieval needed for Spot14 staining. **E**) Enlarged image of the boxed area depicted in D.

Scale bars represent: 1mm (A), 50μm (B, C, D), and 20μm(E).

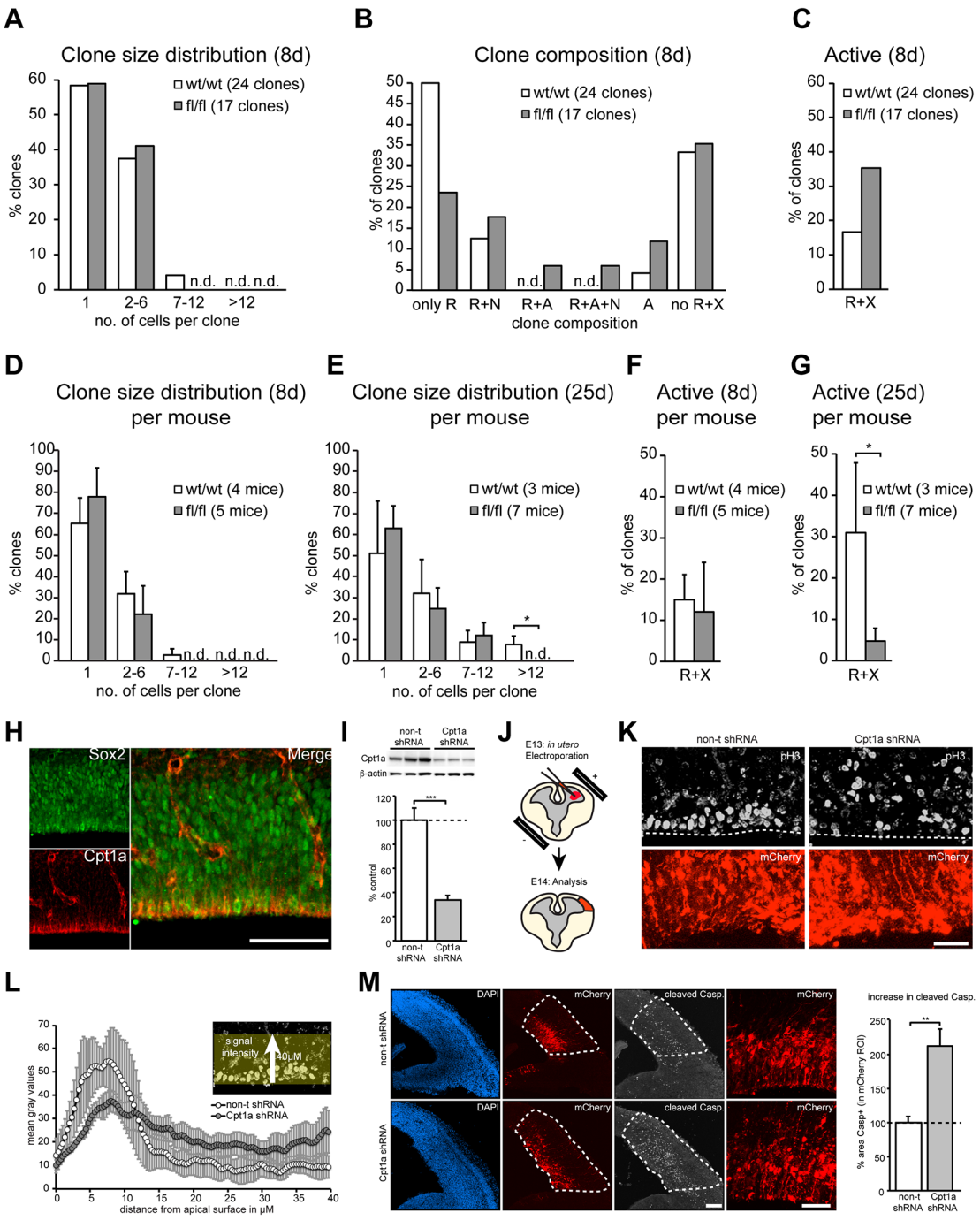

Figure S4 (related to Figure 4): Cpt1a is required for proper neurogenesis in the adult and during development. A) Conditional Cpt1a knockout in adult quiescent NSPCs, by crossing Cpt1a flox/flox mice with Spot14-driven Cre recombinase mice and ROSA YFP reporter mice. Clonal analysis early after TAM

induction (8 days after the first injection) does not yet reveal significant differences in clone size in the Cpt1a-cKO flox/flox mice compared to Cpt1a-cKO wt/wt littermates. **B)** Detailed clone composition analysis shows no significant differences at 8 days after induction, although there was a small decrease in clones containing only R. **C)** The number of active clones early after deletion of Cpt1a is not different between Cpt1a-cKO flox/flox mice compared to Cpt1a-cKO wt/wt littermates despite a small, but non-significant (n.s.) increase (p = 0.17) in active clones containing a radial glia-like cell (R) and any kind of progeny (X) in Cpt1a-cKO mice. **D)** Clone size distribution 8 days after induction, analyzed per mouse instead of per clones (mean ± SEM). Similar to the data shown in A, there is no significant difference at that timepoint. **E**) Clone size distribution 25 days after induction, analyzed per mouse instead of per clones (mean ± SEM). Similar to the data shown in Fig. 4B, there is a significant reduction in the number of large clones in Cpt1a-cKO flox/flox mice compared to Cpt1a-cKO wt/wt littermates. **F)** The number of active clones analyzed per mouse instead of per clones (mean + SEM) does not reveal a significant difference 8 days after induction. **G**) The number of active clones analyzed per mouse instead of per clones (mean ± SEM) at 25 days after induction shows a significant reduction in Cpt1a-cKO flox/flox mice compared to Cpt1a-cKO wt/wt littermates, similar to the data shown in Fig. 4D. **H**) During development, Cpt1a is expressed in the ventricular zone, where NSPCs reside and give rise to newborn neurons. Shown is a representative confocal image (maximum projection) of an E14 wildtype mouse embryo brain stained against Cpt1a (cytoplasm) and Sox2 (nuclei). **I)** A

shRNA targeting Cpt1a was tested for knockdown efficiency compared to a non-targeting control shRNA. All constructs also contain a mCherry reporter sequence. Shown is a representative Western blot of the endogenous Cpt1a levels in Hepa1-6 cells 48h after shRNA-transfection and the corresponding loading control (β-actin). The bar graph shows the quantification of Cpt1a levels normalized to β-actin (mean ± SEM). **J)** ShRNA-mediated Cpt1a knockdown *in vivo* by *in utero* electroporation. Shown is a scheme of the experimental approach: ShRNA constructs were injected into the ventricle of E13 mouse embryos and current was applied to transfect cells in the ventricular zone. Embryos were analyzed one day later (E14) by immunohistochemistry. **K)** Representative images of embryonic brain sections after *in utero* electroporation with a non-targeting shRNA and a shRNA against Cpt1a, both expressing mCherry. Staining against the proliferation marker phospho-histone 3 (pH3) reveals reduced proliferation at the apical surface, where radial glia divide, and a general disorganization of the ventricular zone. **L)** Quantification of the pH3 intensity from the apical surface 40µm into the ventricular zone. **M)** Representative images of embryonic brain sections after *in utero* electroporation of the different shRNA-constructs described in D. Dotted lines show the transfected areas in the cortex marked by mCherry expression. Staining against the apoptotic marker cleaved Caspase-3 reveals massive cell death upon knockdown of Cpt1a, suggesting that FAO is also required for proper neurogenesis during development. Enlarged images of the mCherry positive transfected areas show the apparent morphological differences between non-

targeting shRNA transfected NSPCs and the NSPCs transfected with the Cpt1a targeting shRNA. **I**) Quantification of the increase in cleaved Caspase 3 positive area upon Cpt1a knockdown *in utero* (mean ± SEM).

Scale bars represent: 50μm (B, M), 20μm (K). ***$p < 0.001$, **$p < 0.01$, *$p < 0.05$.

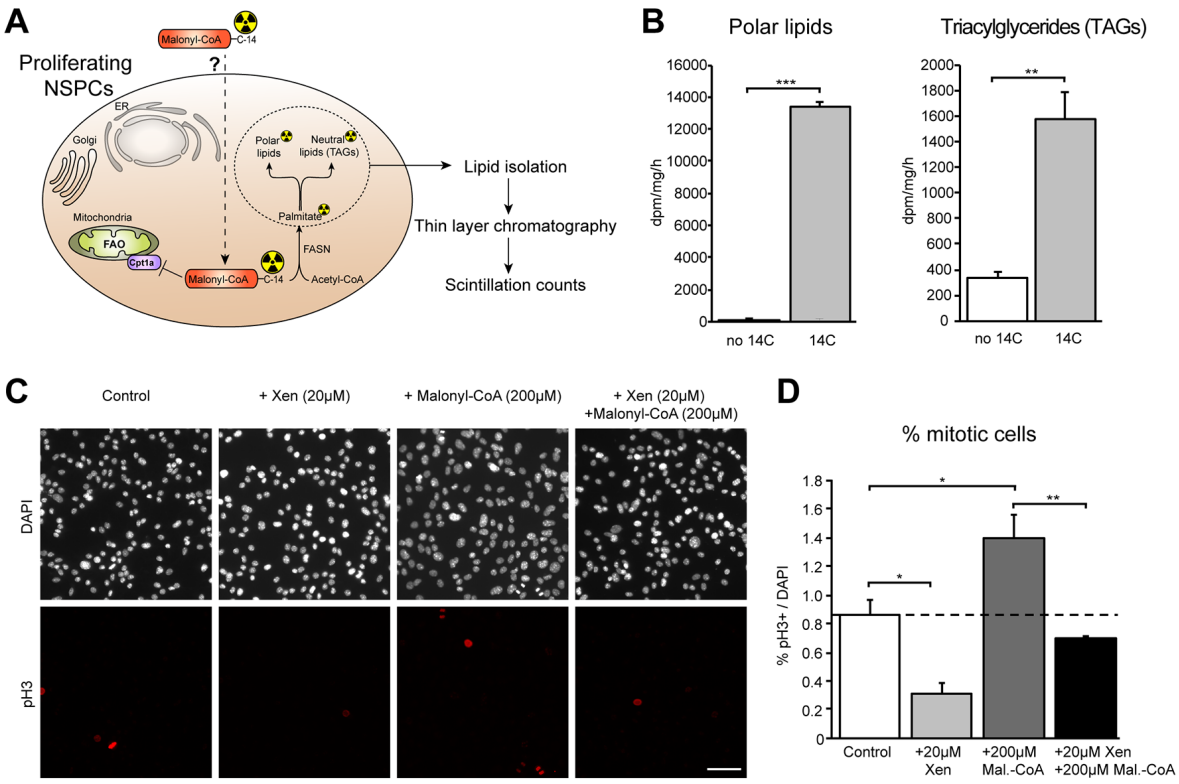

Figure S5 (related to Figure 5): Exogenously applied malonyl-CoA is incorporated into new lipids and increased proliferation upon malonyl-CoA exposure in quiescent NSPCs is at least partially regulated by an increase in FASN-dependent *de novo* lipogenesis. A) Scheme of the experimental procedure to detect whether exogenously applied malonyl-CoA can be used by NSPCs. Radioactively labeled malonyl-CoA (^{14}C-malonyl-CoA) was applied together with non-labelled malonyl-CoA (100μM) to proliferating NSPCs for 48h. Intracellular lipids were isolated, separated by thin layer chromatography and their radioactivity was measured by scintillation counts. **B**) Both in the polar lipid

fraction (containing the phospholipids) and in the neutral lipid fraction (containing triacylglycerides), significantly higher radioactivity (decay per minute, dpm) was detected in the samples incubated with ^{14}C-malonyl-CoA, indicating that exogenously applied malonyl-CoA is taken up and integrated into newly synthesized lipids in NSPCs. **C**) NSPCs were replated after fully established quiescence in quiescence medium containing either vehicle, the FASN inhibitor Xenical (Orlistat, 20 μM), malonyl-CoA (200 μM) or both Xenical and malonyl-CoA (20 μM and 200 μM). **D**) The number of mitotic cells was analyzed 3 days later by pH3 staining. Inhibition of FASN significantly reduced the remaining small percentage of mitotic cells, whereas malonyl-CoA significantly increased proliferation. Xenical abolished the pro-proliferative effect of malonyl-CoA when applied together with malonyl-CoA. This suggests that increased proliferation of quiescent NSPCs is at least partially dependent on FASN-driven *de novo* lipogenesis. Shown are representative images of indicated doses (A) and the quantification of proliferating cells (B) (mean ± SEM).

Scale bar represents 50μm. ***$p < 0.001$, **$p < 0.01$, * $p < 0.05$.

EXTENDED DATA TABLES

Table 1. Listed are the normalized abundances of proteins detected in the mass spectrometric comparison of proliferating and quiescent NSPCs.

Table 2. Listed are the normalized abundances of significantly and at least two-fold changed proteins, belonging to different GO processes.

Table 3. Listed are the primers used for qPCR.

SUPPLEMENTAL EXPERIMENTAL PROCEDURES

RESOURCES TABLE

REAGENT or RESOURCE	SOURCE	IDENTIFIER
Antibodies		
mouse anti-pH3	Abcam	#14955
mouse anti-Cpt1a	Abcam	#ab128568
rabbit anti-Ki67	Novocastra	#NCL-Ki67p
chick-anti-GFP	Aves	#GFP.1020
goat anti-Sox2	Santa Cruz	#sc17320
mouse anti-Nestin	BD Biosciences	#556309
goat anti-DCX	Santa Cruz	#sc 8066
mouse anti Map2ab	Sigma	#M2320
chick anti-GFAP	Aves	#GFAP
mouse-anti GFAP	Sigma	#032M4779
rabbit anti-Spot14	Abcam	#Ab56193
rabbit anti-cleaved Caspase-3	Cell signaling	#Asp175
rabbit anti-dsRed	Living colors	#632496
mouse anti-beta-actin	Sigma	#A2228
Mitotracker Deep red	Invitrogen	#M22426
DAPI	Sigma	#D9542
Biological Samples		
Chemicals, Peptides, and Recombinant Proteins		
Tamoxifen	Sigma	#T5648
Corn-oil	Sigma	# C8267
N2 supplement	Gibco	#17502048
hEGF	Peprotech	#AF-100-15-500ug
hFGF basic	Peprotech	#100-18B-500ug
antibiotic/antimycotic	Thermo Scientific	#15240-062
Heparin	Sigma	#H3149-50KU
Poly-ornithine	Sigma	#P36655
Laminin	Sigma	# L2020
mouse BMP4	R&D Systems	#5020-BP-010
Trypsin	Gibco	#15090
Versene	Gibco	#15040-033
Ovomucoid trypsin inhibitor	Sigma	#T6522
DNAse I type IV	Sigma	#D5025-15 KU
Malonyl-CoA	Sigma	#M4263
Etomoxir	Sigma	#E1905
Xenical (Orlistat)	Roche	Xenical 120 mg
Hoechst 33342	Invitrogen	#H3570

Wy14643	Enzo Life Sciences	# BML-GR200-0250
Lipofectamine-2000	Thermo Scientific	#11668019
Complete EDTA-free proteinase Inhibitor tablets	Roche	#11873580001
[9,10-^{3}H(N)]palmitic acid	PerkinElmer	#NET043001MC
[1-14C]palmitic acid	PerkinElmer	#NEC075H050UC
fatty acid-free albumin	Sigma	#A8806
sodium palmitate	Sigma	#P9767
L-carnitine	Sigma	#C0158
C13-labelled palmitate	Cambridge Isotope Laboratories Inc.	#CLM-3943
DOWEX 1X2 chloride form resin (200-400 mesh)	Sigma	#217395
IRGASAFE Plus, scintillation liquid	Zinser Analytic	#1003100
Critical Commercial Assays		
Click-iT EdU Imaging Kit	Invitrogen	#C10338
BCA Protein determination	Pierce	#23225
BC assay	Uptima	#FT-40840A
Vectastain ABCKit	Vector Laboratories	#PK-6100
Nucleo Spin RNAII Kit	Macherey & Nagel	#740955
Superscript III Kit	Invitrogen	#18080093
Deposited Data		
Raw and analyzed Proteomics Data	This paper	PXD005598
Experimental Models: Cell Lines		
Mouse: primary dentate gyrus NSPCs	(Ray and Gage, 2006)	N/A
Mouse: liver hepatome cells (Hepa1-6 cells)	Leibniz Institute DSMZ	#ACC 175
Experimental Models: Organisms/Strains		
Mouse: Tg(Cpt1a-EGFP)IP41Gsat/Mmucd	MMRRC	# 030281-UCD
Mouse: C57BL/6JRj wildtype mice	Janvier	#C57BL/6JRj
Mouse: Cpt1a cKO mice	(Schoors et al., 2015)	N/A
Mouse: Spot14CreERT2 mice (S14iCre)	(Knobloch et al., 2013)	N/A
Mouse: B6.129X1-*Gt(ROSA)26Sor*$^{tm1(EYFP)Cos}$/J (R26YFP)	Jackson laboratory	#006148
Mouse: S14iCre x Cpt1a cKO x R26YFP	This paper	N/A
Recombinant DNA		
Cpt1a shRNA1 5'-3': CCGGCGTGAGGAACTCAAACCTATTCTCGAGAATAGGTTTGAGTTCCTCACGTTTTTG (targeting Cpt1a from nucleotide 949-969)	This paper	N/A
Non-targeting shRNA 5'-3': TCCTAAGGTTAAGTCGCCCTTTCAAGAGAAGGGCGACTTAACCTTAGGTTTTTTC	This paper	N/A
LentiLox3.7 U6 shRNA (pLL3.7)	Addgene	#11795
LentiLox3.7 mcherry U6 shRNA	(Knobloch et al., 2013)	N/A

Sequence-Based Reagents		
Primers for qPCR	This paper	See Table 3
Software and Algorithms		
Imaris	Bitplane	www.bitplane.com
ImageJ	NIH Image	*https://imagej.net/*
Free-D	Free-D	http://free-d.versailles.inra.fr/
Photoshop	Adobe	www.adobe.com
Progenesis QI for proteomics	Nonlinear Dynamics	http://www.nonlinear.com/progenesis/qi-for-proteomics/
Scaffold 4	Proteome Software	http://www.proteomesoftware.com/products/scaffold/
Metacore 6.24 build 67895	Thomson Reuters	www.thomsonreuters.com
Xcalibur software	Thermo Scientific	OPTON-30487
Other		

CONTACT FOR REAGENT AND RESOURCE SHARING

Further information and requests for resources and reagents should be directed to and will be fulfilled by the Lead Contact Sebastian Jessberger (jessberger@hifo.uzh.ch)

EXPERIMENTAL MODEL AND SUBJECT DETAILS

Animals

Mice were kept in a specific pathogen free (SPF) animal facility according to the guidelines of the Federation of European Laboratory Animal Science Associations (FELASA), where persons entering the facility must wear protective cloths, facemasks, hairnets and gloves after crossing a barrier. Mice were kept with littermates under a 12h dark/light cycle in individually ventilated cages and with *ad libitum* access to food and water. The *Cpt1a-EGFP* reporter mouse line (STOCK Tg(Cpt1a-EGFP)IP41Gsat/Mmucd) was generated by the Mutant Mouse Regional Resource Centers (MMRRC). Founders were cryo-resuscitated and bred thereafter with C57BL/6JRj wildtype mice (Janvier Labs, France). Genotyping was performed using 5'-CTGGTGCCAGGCTTCTAA-3' forward and 5'-TAGCGGCTGAAGCACTGCA -3' reverse primers. Six females were used for histological analyses at the age of two months. For in utero electroporation experiments, time-mated C57BL/6JRj female mice were obtained from Janvier Labs (France). Cpt1a cKO mice (Schoors et al., 2015) were embryo-transferred

through C57BL6/J (Jackson laboratory) and kept thereafter on a heterozygous level by crossing them with C57BL/6JRj (Janvier Labs, France). They were crossed with Spot14CreERT2 mice (S14iCre (Knobloch et al., 2013)) and ROSA26 YFP reporter mice (R26YFP, B6.129X1-*Gt(ROSA)26Sor*$^{tm1(EYFP)Cos}$/J, kept for more than 10 generations on a C57BL/6J background) to obtain S14iCre +/-; Cpt1a cKO wt/wt; R26YFP fl/wt and S14iCre +/- ; Cpt1a cKO fl/fl; R26YFP fl/wt littermates. Breedings were set up in a way that all the genotypes were generated within one litter and that several litters were born within one week. Littermates were assigned to the different groups based on genotype. Due to low recombination efficiency, Cre-mediated recombination was induced by five intraperitoneal injections of tamoxifen on five consecutive day (Sigma, 180mg/kg, dissolved in cornoil) at the age of six to seven weeks. All animals received tamoxifen. Animals were perfused either eight days or twenty-five days after first tamoxifen injections. For the eight day timepoint, one male and three females of S14iCre +/-; Cpt1a cKO wt/wt; R26YFP fl/wt and one male and five females of S14iCre +/- ; Cpt1a cKO fl/fl; R26YFP fl/wt were induced. One S14iCre +/- ; Cpt1a cKO fl/fl female had to be excluded from the analysis, as no YFP positive cells were detected in the DG. For the twenty five day timepoint, two males and three females of S14iCre +/-; Cpt1a cKO wt/wt; R26YFP fl/wt and one male and six females of S14iCre +/- ; Cpt1a cKO fl/fl; R26YFP fl/wt were induced. Two S14iCre +/-; Cpt1a cKO wt/wt; R26YFP fl/wt (one male, one female) had to be excluded from the analysis, as no YFP positive cells were detected in the DG.

All animal experiments were performed according to Swiss regulatory standards and approved by the Veterinary office of the Canton of Zurich.

Cells

Primary adult mouse DG (mDG) NSPCs were obtained and cultured as previously described (Knobloch et al., 2013; Ray and Gage, 2006). In brief, DGs from eight female C57BL6/J (Jackson laboratory) were subdissected and processed as described (Ray and Gage, 2006). Early passages were frozen and kept in liquid nitrogen. Experiments were performed with cells up to passage 20. Mycoplasma tests were performed on a regular base to verify that cells were mycoplasma free. Mouse liver hepatome cells (Hepa1-6 cells) were grown as suggested by the provider, Leibnitz Institute DSMZ (Catalogue code: ACC 175).

Plasmids

Cpt1a shRNA sequence was designed using the RNAi Consortium hairpin candidate sequences selection (www.broadinstitute.org/rnai/trc) against mouse Cpt1a (NM_013495). The sequences of the oligonucleotides used are as follows:

Cpt1a shRNA1 5'-3':

CCGGCGTGAGGAACTCAAACCTATTCTCGAGAATAGGTTTGAGTTCCTCAC GTTTTTG (targeting Cpt1a from nucleotide 949-969)

non-targeting shRNA 5'-3':

TCCTAAGGTTAAGTCGCCCTTTCAAGAGAAGGGCGACTTAACCTTAGGTTTT TTC

The shRNA knockdown constructs (derived from LentiLox3.7) were cloned to express mCherry under the CMV promoter and shRNAs under the U6 promoter.

METHOD DETAILS

Cell culture

Primary mDG NSPCs were kept as monolayer cultures in DMEM/F12 Glutamax medium supplemented with N2 (Invitrogen), human EGF (20 ng/ml), human basic FGF-2 (20 ng/ml, Peprotech) and Heparin (5mg/ml, Sigma). Medium contained an antibiotic/antimycotic (Anti-Anti, Thermo Fisher Scientific). This proliferation medium was changed every 2-3 days.

For all experiments involving quiescence induction and/or immunocytochemistry, cells were plated on glass coverslips or multi-well cell culture dishes coated with Poly-L-ornithine (Sigma, 10µg/ml for plastic, 50µg/ml for glass) and Laminin (Invitrogen, 5µg/ml). All experiments were done with a minimum of 3 coverslips per condition.

Quiescence was induced as previously described (Martynoga et al., 2013; Mira et al., 2010). In brief, exchanging EGF with recombinant mouse BMP4 (RnD Systems) results in a significant drop in proliferation over the course of 3 days with almost no more proliferation detectable after 3 days. This artificial quiescence is fully reversible after replating NSPCs in proliferation medium. For all quiescence experiments, cells were plated in proliferation medium (~40’000

cells/cm^2) and switched the next day to quiescence medium, which was composed of DMEM/F12 Glutamax supplemented with N2, human basic FGF-2 (20 ng/ml), Heparin (5mg/ml) and BMP4 (50ng/ml, BMP4 stock dissolved in 4mM HCL/PBS/0.5%BSA). Cells were kept for a minimum of 3 days in quiescence medium before fixation or harvest. For comparisons with proliferating NSPCs, cells were plated in parallel at a lower density (~14'000 cells/cm^2) and kept in proliferation medium over the same time period as the quiescent NSPCs, with medium change every 2 days. To reverse quiescence, NSPCs were collected after 3 days of quiescence and replated in fresh proliferation medium (~50'000 cells/cm^2). To compare the proliferation rate of formerly quiescent NSPCs to cells that had not entered quiescence, proliferating NSPCs that were grown in parallel were also replated in fresh proliferation medium at slightly lower density (~30'000 cells/cm^2). For extended reversal of quiescence (6 days proliferation medium after quiescence), cells were replated as described above and split again 3 days later. For the experiments were effects of compounds on quiescence were tested cells were treated as followed: full quiescence was established as described above for 3 days, cells were washed off the plate with old medium, trypsinized with 2.5% Trypsin diluted to .05% in Versene (Invitrogen) and blocked with a trypsin Inhibitor Mix (L-15 medium, 0.1% ovomucoid trypsin inhibitor (Sigma), 0.05% BSA and 0.01% DNAse I type IV). Cells were spun down in PBS, counted and plated onto freshly coated plates in fresh quiescence medium (~220'000 cells/cm^2). 100 µM or 200 µM Malonyl-CoA (Sigma) was added as outlined in the

corresponding figures. 20 μM Orlistat (Xenical, Roche) was used as previously described (Knobloch et al. 2013).

For cell cycle analysis, two different methods were used. Cells were either harvested and stained in a fluorochrome solution (0.1% sodium citrate, 0.1% Triton X-100 and 50mg/L Propidium iodide) for 1h at 4°C or incubated live for 30min at 37°C (in the cell culture incubator) with Hoechst 33342 (Invitrogen, 1: 2000) Flow cytometry was performed on a LSRII instrument (Becton Dickson) and data were analysed using FlowJo software (Tree Star, Inc.). For Cpt1a inhibition, various doses of Etomoxir (50-200μM, Sigma) or Malonyl-CoA (100-200μM, Sigma) were added to the medium as outlined in the main figures.

The PPARα agonist Wy14643 (Enzo Life Science) was dissolved in 100% EtOH and 100μM was added to proliferating NSPCs for 48h. The same amount of 100% EtOH was added to proliferating NSPCs as a control. After 48h, cells were either collected for RNA isolation (see below) or incubated with EdU (5-ethynyl-2'-deoxyuridine, Invitrogen, 10μM, 1h pulse at 37°C in cell culture incubator), fixed and processed for immunocytometry as described below.

To assess the knockdown efficiency of the Cpt1a-shRNA construct, mouse liver hepatoma cells (Hepa 1-6 cells) that naturally express high Cpt1a levels were transfected with the 2 different constructs, using lipofectamine-2000 (Thermo Fisher). 48h later, cells were lysed and analyzed by Western blot as described below.

Time-lapse imaging and analysis

For time-lapse imaging, NSPCs were plated as described above in coated plastic cell culture plates in triplicates for each condition. Cells were placed in a heated and CO_2-controlled chamber of an inverted microscope (Zeiss, Axio Observer) and 4-6 adjacent areas were imaged every 4h. Stitched phase contrast images were analysed using ImageJ. Several processing steps (bandpass filtering, Gaussian blurs, thresholding) were used to automatically analyze the area covered by cells.

Proteomics analysis

Sample preparation

Proliferating and quiescent NSPCs were cultured as described above on coated 10cm plates. Prior to protein extraction cells were washed twice using 4°C cold PBS (Life Technology). Cells were lysed using 300µl lysis buffer (150mM NaCL, 50mM Tris, 5mM EDTA, 20mM N-Ethylmaleimide, 2mM PMSF, 1x Complete EDTA-free proteinase Inhibitor tablets, ROCHE). Lysates were collected in precooled screw cap tubes (Sarstedt). Lysates were supplemented with 1.7% Triton (Sigma) and 1% Chaps (Sigma) and incubated for 1h with end over end rotation at 4°C. Lysates were cleared by centrifugation at 17000g for 10min and protein concentration was determined using Protein DC assay (Biorad) following the Manufacturer's instructions. 100µg protein was precipitated twice by methanol/chloroform precipitation and protein pellets were resuspended in SDS lysis buffer (4% (w/v) SDS, 100mM Tris/HCL pH 8.2, 0.1M DTT) and stored at -

80°C. Protein samples were processed using a modified protocol by filter aided sample preparation (FASP) (Wisniewski et al., 2009). In brief, samples were incubated for 5 min at 95°C with 700 rpm shaking on a head block (Eppendorf), followed by 10min sonication. Protein concentration was measured using a Qubit 2.0 Fluorometer (Thermo Fisher Scientific) following the Manufacturer's instructions and 20µg protein per sample was used for further processing. Samples were mixed with 200µl 8 M urea in 100mM Tris/HCl pH 8.2 (UA) and loaded to Microcon-30 centrifugal filter units (Millipore), washed once with 200µl UA, alkylated with 100µl 50mM Iodoacetamide and incubated for 1min at 600rpm in a Thermo mixer (Eppendorf). Filter units were washed 3x with 100µl UA and 2x with 100µl 0.5M NaCl. Filter units were then transferred to new collection tubes and incubated with 120µl TEAB with trypsin (1:50 (w/w) ratio of trypsin to protein) (Promega) overnight in a wet-chamber. If not otherwise stated, all centrifugation steps were performed for 20 min at RT. Samples were collected and acidified to a final concentration of 0.5% TFA followed by Solid Phase Extraction (SPE) C18 clean up. Finisterre SPE columns (100mg/1ml; WICOM International) were pre-wetted with 1ml 100% MeOH and cleaned with 1ml of 60% ACN, 0.1% TFA before equilibration with 3% ACN, 0.1% TFA. The volume of peptide containing samples was adjusted to 500µl with 3% ACN 0.1% TFA and loaded onto SPE columns and washed twice with 1ml of 3% ACN, 0.1% TFA. Peptides were eluted with 60% ACN, 0.1% TFA, completely dried (Centrivap, Labconco) and dissolved in 3% ACN; 0.1% FA). Prior to measurements, peptide

samples were supplemented 1:40 with Retention Time Normalization Peptides (BIOGNOSYS).

LC MS/MS analysis

All data was acquired on an Orbitrap Fusion Tribrid mass spectrometer (Thermo Scientific, San Jose, Ca), which was connected to an Easy-nLC 1000 HPLC system (Thermo Scientific). 4µl of the peptide samples were loaded onto a frit column (inner diameter 75µm, length 15 cm) packed with reverse phase material (C18-AQ, particle size 1.9µm, pore size 120 Å, Dr. Maisch GmbH, Germany), and separated at a flow rate of 250nl per min. Solvent composition of buffer A was 0.1% formic acid in water, and buffer B contained 0.1% formic acid in acetonitrile. The following LC gradient was applied: 0 min: 3% buffer B, 50 min: 25% B, 60 min: 32% B, 70 min: 97% B, 80 min: 97% B. Survey scans were recorded in the Orbitrap mass analyzer in the range of m/z 300-1500, with a resolution of 60000 and a maximum injection time of 100 ms. Higher energy collisional dissociation (HCD) spectra were acquired in the ion trap, using a maximum injection time of 35 ms. The precursor ion isolation width was set to m/z 2.0, and a normalized collision energy of 30% was used. Charge state screening was enabled, and charge states 2-6 were included. No threshold for signal intensities was applied, and precursor masses already selected for MS/MS acquisition were excluded for further selection during 45 s.

MS data processing

Raw files were processed with Progenesis QI for proteomics (Nonlinear Dynamics). In brief, runs were aligned to a reference sample containing the most comprehensive number of peptide ions to compensate for between run differences in the retention time. Only peptide ions with a charge state of two, three and four were included into the analysis, default normalization was performed. For peptide identification, up to three tandem mass spectra per peptide ion were exported to a Mascot generic file (mgf) with fragment ion count limited to 200 and deisotoping as well as charge deconvolution was applied. Mascot (2.4.1) was used for searching a target-decoy mouse database downloaded from uniprot (03/01/2015), as decoys protein sequences were reversed and concatenated to the forward database. Parameters were set as following: peptide tolerance +-10ppm, MS/MS tolerance +-0.7DA, variable modifications: Acetyl (Protein N-term), Carbamidomethyl (C), Gln → pyro Glu (N-term), N-Ethylmaleimide, N-Ethylmaleimide + water, oxidation (M). Resulting Mascot dat-files were imported into Scaffold 4 (Proteome Software) and the false discovery rate (FDR) for peptides was set to 0.01, for proteins to 0.05 respectively. The Scaffold Spectrum Report was re-imported into Progenesis and relative quantitation using non-conflicting peptides was performed. Decoy hits were excluded and protein quantitation and statistics were exported as .csv files.

Gene Ontology analysis

Gene names, p-values and normalized protein abundance were exported to Metacore 6.24 build 67895 (Thomson Reuters). Members corresponding to the

GO terms: GO:0019395, GO:0006633, GO0006096, GO:0006098, GO:0008652, GO:0006099, GO: 0022904, GO:0006754 were exported. Changes in protein abundances were represented as histograms using Prism 6 (Graphpad).

Radioactive FAO measurements

Radioactively labeled palmitic acid ([9,10-^{3}H(N)]palmitic acid (32Ci/mmol, NET043001MC) and [1-14C]palmitic acid (56.1mCi/mmol, NEC075H050UC) were purchased from Perkin Elmer.

FAO of [9,10-^{3}H(N)]palmitic acid was assessed by the production and release of tritiated water according to a modified procedure (Djouadi et al., 2003). Proliferating and quiescent NSPCs were grown in 24-well plates as described above and the tritiated water release experiments were performed in triplicate (3 wells per sample/condition). A 500µM stock solution of [9,10-^{3}H(N)]palmitic acid was prepared by complexing labeled and unlabeled palmitate to fatty acid-free albumin (PAA) as follows: 0.1mCi of ^{3}H-palmitic acid and 130µl of 50mM palmitate (Sigma, dissolved in 100% ethanol) were mixed and dried under N_2. 13ml of BSA (2.5mg/ml) in PBS were added to the dried palmitate, vortexed vigorously and incubated in a shaker at 37 °C overnight. The palmitate/BSA stock solution was stored at -20 °C. The reaction was initiated by replacing the culture medium with 200µl of the reaction mixture. The reaction mixture was prepared by diluting the palmitate/BSA stock solution four-fold with cell culture medium and contained 0.385µCi [9,10-^{3}H(N)]palmitic acid and 125µM sodium palmitate and 1mM L-carnitine (Sigma). The culture plate was wrapped in foil to

avoid evaporation and incubated for 4h at 37 °C. In some experiments, 100µM Etomoxir (Sigma), an inhibitor of mitochondrial FAO, was added to wells as a negative control. At the end of the incubation period, the reaction mixture from each well was transferred to a tube containing 200µl of cold 10% trichloroacetic acid (TCA) to stop the reaction. The tubes were centrifuged at 2200 *g* at 4 °C for 10 min. The radioactive product ^3H_2O was eluted with 1.7ml deionized water and quantified by scintillation counting. Aliquots of supernatants (350µl) were removed and mixed with 55µl of 6M NaOH to neutralize the TCA. The total volume was applied to an ion-exchange column packed with 2.4ml of 0.37g/ml DOWEX 1X2 chloride form resin (200-400 mesh, Sigma). After the sample completely entered the column, the radioactive product ^3H_2O was eluted with 1.7ml deionized water directly into a scintillation vial, mixed with 5ml of scintillation liquid (IRGASAFE Plus, Zinsser Analytic) and quantified by scintillation counting (Beckman Coulter LS 6500 Multi-Purpose Scintillation Counter). For the calculation of the specific radioactivity of the reaction mixture, 20µl of the reaction mixture were mixed with 1.5ml H_2O and 5 ml scintillation liquid. After removal of the reaction mixture cells were washed with PBS and lysed in 0.1M NaOH for protein determination using the BCA procedure (Pierce). The FAO of [1-^{14}C]palmitic acid was assessed by the production and release of $^{14}CO_2$ according to a modified procedure of Huynh et al. (2014).

A 2.5mM stock solution of [1-^{14}C]palmitic acid was prepared by complexing labeled and unlabeled palmitate to fatty acid-free albumin as follows: the amount of radiolabeled palmitic acid in ethanol required to assay each

sample with 0.2µCi per well was dried under N_2. The dried palmitate was resolubilized in the appropriate amount of 7% BSA/2.5mM palmitate warmed to 37 °C to get a stock solution of 7% BSA/2.5mM palmitate/0.01µCi/ml 14C-palmitate. The reaction mixture was prepared by diluting the palmitate/BSA stock solution 25-fold with cell culture medium and contained 0.2µCi [1-^{14}C]palmitic acid and 100µM sodium palmitate and 1mM L-carnitine in 500µl medium. Cells were seeded in 24-well plates and the experiments were performed in quadruplicates (4 wells per sample/condition). The reaction was initiated by replacing the culture medium with 500µl of the reaction mixture. The culture plate was sealed with parafilm to avoid evaporation and incubated for 2.5h at 37 °C. In some experiments, 100µM Etomoxir was added to wells as a negative control. During the incubation, acidification vials with a $^{14}CO_2$ trap were prepared by adding 200µl of 1M perchloric acid (Sigma) to tubes that contained a Whatman filter paper disc inside the cap that had been wetted with 20µl of 1M NaOH. At the end of the incubation, 400µl of the reaction mixture was added into an acidification vial to stop the reaction and incubated for 1h at room temperature. The paper disc was transferred to a scintillation vial, mixed with 5ml of scintillation liquid and quantified by scintillation counting. After removal of the reaction mixture cells were washed with PBS and lysed in 0.1M NaOH for protein determination using the BCA procedure (Pierce).

Radioactive malonyl-CoA incorporation measurements

Cells were incubated with 0.5 µCi [2-^{14}C]malonyl-CoA (55 mCi/mmol; Cat. No. ARC 0528, American Radiolabeled Chemicals, USA) and 100 µM malonyl-CoA. After incubation, the cells were rinsed three times with PBS, and lipids were extracted with hexane:isopropanol (3:2). Manipulative losses of lipids were accounted for by addition of a known amount of [1,2-^{3}H(N)]cholesterol (Cat. No. NET139250UC; PerkinElmer) as internal standard. After lipid extraction cells were lysed in 0.1 M NaOH for protein determination using the Pierce BCA Protein Assay Kit (Cat. No. 23227, Thermo Scientific, Rockford, IL, USA). Malonyl-CoA incorporation into specific lipids was analyzed after separation of lipids by thin-layer chromatography. Therefore, organic phases were evaporated to dryness under a nitrogen stream. Lipids were resuspended in chloroform and spotted together with appropriate lipid standards on silica gel 60 F_{254} plates (Cat. No. 1.05715.0001; Merck, Darmstadt, Germany). For separation of neutral lipids, plates were developed in heptane:diethylether:acetic acid (90:30:1) as solvent. Lipid samples and standards were visualized by iodine vapor. The lipid fractions were scraped from the plate, mixed with 5 ml of scintillation liquid (IRGASAFE Plus, Zinsser Analytic, Cat. No. 1003100) and quantified by scintillation counting (Beckman Coulter LS 6500 Multi-Purpose Scintillation Counter). Values were normalized for sample protein content.

In utero electroporation and tissue preparation

In-utero electroporation of mouse embryos (embryonic day 13, E13) from time-mated C57BL/6JRj female mice was carried out as described previously (Asami et al., 2011). In brief the shRNA plasmid DNA (Cpt1a-shRNA1 or non-targeting shRNA; final concentration 0.5-0.7µg/µl) was targeted into the ventricular wall by repeated electrical pulses (ElectroSquireporator T830, Harvard Apparatus). After 24h (corresponding to developmental stage E14), electroporated brains were dissected in ice cold PBS and fixed in phosphate buffered 4% paraformaldehyde (PFA; Sigma) on 4°C for 2 hrs. After rinse in PBS, embryonic brains were dehydrated in 30% sucrose (in PBS), embedded and frozen in OCT compound (Tissue-Tek; Sakura), and cut in slices of 30µm thickness using a Cryostat (Microm).

Tissue preparation, Immunohistology and Immunocytochemistry

Mice were transcardially perfused with 0.9% saline solution followed by 4% PFA solution. Brains were taken out and post-fixed overnight at 4°C in 4% PFA. After dehydration in 30% sucrose, 40µm thick free-floating sections were cut on a microtome (Leica). Sections were blocked for 1h with blocking buffer (0.25% Triton-x, 3% donkey serum in PBS) and subsequently incubated with primary antibodies in blocking buffer at 4°C overnight. Sections were washed 3x with PBS and incubated for several hours at room temperature with secondary antibodies in blocking buffer. Nuclei were stained with DAPI. After another 3 washes with PBS sections were mounted (Shandon Immu-mount, Thermo

Scientific). For Spot14 stainings, section were pretreated for 5h at RT with a buffer containing 1%Triton-x and 3% donkey serum, followed by 3 days primary antibody incubation in blocking buffer. An additional enhancement step with a biotinylated secondary antibody followed by a streptavidin-coupled fluorophore was used. Cells were fixed with 4%PFA (37°C, fixed at RT for 20min), washed 3x with PBS and incubated in blocking buffer for 1h. Antibody stainings were done overnight at 4°C, secondary antibodies were incubated 2-4h at RT.

The following primary antibodies and dilutions were used: mouse anti-pH3 (1:1000, Abcam), mouse anti-Cpt1a (1:500, Abcam), rabbit anti-Ki67 (1:500m, Novocastra), chick-anti-GFP (1:500, Aves), goat anti-Sox2 (1:500, Santa Cruz), mouse anti-Nestin (1:500, BD Biosciences), goat anti-DCX (1:250, Santa Cruz), mouse-anti GFAP (1:500, Sigma), rabbit anti-Spot14 (1:250, Abcam), rabbit anti-cleaved Caspase-3 (1:500, Cell signaling), rabbit anti-dsRed (1:500, Living Colors), mouse anti-Map2ab (1:500, Sigma), chick anti-GFAP (1:500, Aves). All secondary antibodies were raised in donkey and used 1:250 (Jackson ImmunoResearch). Mitotracker Deep red was added to cells for 1h at 37°C (100nM, Invitrogen), DAB staining was done according to the manufacturer's protocol (Vectastain ABCKit, Vector Laboratories). EdU staining was performed before antibody incubation using the Click-iT EdU Imaging Kit (Invitrogen).

Image acquisition and analysis

Images of cell stainings were acquired using an Epifluorescent microscope (Zeiss Axiovert Observer). Images were analysed using ImageJ with customized

macros for automated detection in a blinded manner. For differentiated cells, confocal microscopy (LSM-700, Zeiss) was perfomed and z-projections were generated for analysis in ImageJ. Images were thresholded, a watershed filter was applied and DAPI positive nuclei were counted with the analyze particle function. To quantify MAP2ab positive cells masks of the MAP2ab channel were generated and DAPI positive nuclei inside the MAP2ab mask were counted using the particle analyzer. Image acquisition and analysis were performed in a blinded manner. For co-localization experiments, confocal microscopy (LSM-700, Zeiss, FV1000; Olympus) was performed. Images of brain tissue were acquired using a Zeiss AxioImager microscope (for DAB stainings) or by confocal microscopy (LSM-700, Zeiss). One-to-two series of sagittal sections (corresponding to a 6th-3rd of the entire brain) were used from 2 months old Cpt1a-EGFP reporter mice (n=3-6) for quantification. To determine the percentage of Sox2 and DCX cells that were Cpt1a-eGFP+, analyses were carried out using both softwares Imaris (Bitplane) and ImageJ software. In Imaris, a surface was first created using either the Sox2 or DCX channel. Subsequently, this surface was used to mask the GFP signal. A snapshot of the maximum projection of each raw channel as well as each masked channel was saved for further import into ImageJ. To demarcate the SGZ, DAPI and DCX images were merged to outline the specified region. Bright Sox2 or DCX positive cells within the SGZ were circled to create region of interests (ROIs). These ROIs were then overlaid onto the masked GFP channel to determine if the Sox2+ or DCX+ cells were Cpt1a-eGFP+. At least 3 sections from 3 different animals were used to count >50 cells for each condition.

The same procedure was used to determine the number of Nestin-positive processes that also were Cpt1a-eGFP+.

For the *in utero* electroporation experiments, images were analyzed in a blinded manner with ImageJ. A region of interest was drawn over the mCherry positive area (stained as described above) from the ventricular zone to the pial surface. This region of interest was then applied to the adjacent sections stained against cleaved Caspase 3. A threshold was set and the %area covered by Caspase-3 positive cells was measured. 4-5 sections per embryo were analyzed (non-targeting n=4 embryos, Cpt1a shRNA1 n=5 embryos). For pH3 quantification, regions with mCherry signal were selected and signal intensity of corresponding adjacent sections stained for pH3 were analyzed with ImageJ. Mean gray values 40μm from the apical surface into the ventricular zone were measured along the electroporated area and plotted in relation to distance. 3-4 sections per embryo were analyzed (non-targeting n=3 embryos, Cpt1a shRNA1 n=4 embryos).

Clonal analysis

Serial 40μm sections of an entire hemisphere per mouse were stained with antibodies against GFP, Sox2 and doublecortin (DCX). All sections containing GFP positive cells were imaged with a 20x confocal microscope (for cellular identification) as well as with a 5x Epifluorescent microscope (for reconstruction). Cell identity was determined in a blinded manner based on the following criteria, similar to what has been previously described (Bonaguidi et al., 2011).

Radial-glia like cell (R): triangular shaped soma in SGZ with radial, arborized process into GCL (sometimes not entirely visible), Sox2 positive, DCX negative.

Neural progeny (N): this group contains non-radial cells (more oval to roundish soma in SGZ with one or more horizontal process, Sox2 positive), progenitor cells (roundish soma in SGZ, DCX positive but without long vertical process yet, sometimes still Sox2 positive) and immature/mature neurons (round soma in GCL with long more or less vertical process, Sox2 negative, usually DCX positive, but sometimes DCX already absent). Astrocytes (A): multi-process containing, star shaped or bushy cell in SGZ/Hilus or GCL.

After cellular identification, clonal reconstruction was done based on the order of sections and based on the 5x overview images, followed by image overlay with the software Free-D (http://free-d.versailles.inra.fr/) and Photoshop (Adobe).

Cells within the same spatial location and not more than 160µm apart in all 3 dimensions were assigned as belonging to a single clone. In the 25d timepoint group, a total of 62 clones were identified from three S14iCre-R26YFP-Cpt1acKO wt/wt mice (two females, one male) and a total of 34 clones were identified from seven S14iCre-R26YFP-Cpt1acKO fl/fl mice (six females, one male). In the 8d timepoint, a total of a total of 24 clones were identified from four S14iCre-R26YFP-Cpt1acKO wt/wt mice (three females, one male) and a total of 17 clones were identified from five S14iCre-R26YFP-Cpt1acKO fl/fl mice (four females, one male).

RT-PCRs

RNA of proliferating, quiescent, re-plated proliferating and formerly quiescent NSPCs (grown as described above) as well as of NSPCs treated with the PPARα agonist Wy14643, control NSCPs and quiescent NSPCs grown in parallel was isolated with the Nucleo Spin RNAII Kit (Macherey & Nagel). cDNA was synthesized using the Superscript III Kit (Invitrogen) according to the manufacturer's protocol. Taqman probes against mouse Cpt1a, Spot14 and β-actin and RT-PCR master mix were obtained from Applied Biosystems and used according to the manufacturer's protocol. Real time PCR and data analysis was performed on an Applied Biosystems 7900HT System. Fold changes were calculated using the deltadelta Ct methods.

For PPARα target gene analysis, qRT-PCR was performed on a Roche LightCycler 480 in LightCycler 480 Multiwell Plate 96. The 20 µl amplification mixture consisted of 2x KAPA SYBR FAST qPCR Mastermix (KAPA Biosystems,) and 4 pmol forward and reverse primers (Microsynth, Switzerland) and approximately 10 ng of cDNA template. Thermal cycling was carried out with a 5 min denaturation step at 95 °C, followed by 45 three-step cycles: 10 sec at 95 °C, 10 sec at 60 °C, and 10 sec at 72 °C. Finally, melt curve analysis was carried out to confirm the specific amplification of a target gene and absence of primer dimers. All reactions were run in duplicate. Relative mRNA amount was calculated using the deltadelta Ct methods. Cyclophilin was used as the invariant control. Results were confirmed with 18S rRNA as the invariant control (data not shown). Primers used are listed in Table S3.

Western Blot

Proliferating and quiescent NSPCs were lysed in RIPA buffer containing protease inhibitors (Complete, Roche). Protein amount was determined with a BC assay (Uptima) and equal amounts of proteins were separated by SDS-PAGE electrophoresis followed by transfer to PVDF membrane (BioRad). Membranes were incubated with mouse anti-Cpta1 (1:2000, Abcam) and mouse anti-beta-actin (1:10'000, Sigma). HRP-conjugated secondary antibodies (Jackson immunoResearch) were used and signal was revealed by enhanced chemiluminescence substrate (ThermoScientific).

Malonyl-CoA and acetyl-CoA measurements

Proliferating and quiescent NSPCs were washed with 75mM ammonium carbonate pH 7.4 and plates were snap frozen with liquid nitrogen. Metabolites were extracted with cold acetonitrile:methanol:water solvent (40:40:20) at -20°C for 10 minutes and an extraction step was repeated once. Samples were centrifuged at 13000rpm for 3 minutes and kept at -80°C. Extracts were dried by vacuum-centrifugation, re-suspended in 50µl water and analyzed by LC-MS/MS on a Thermo Quantum Ultra instrument equipped with a Waters Acquity UPLC (Buescher et al., 2010). Data analysis was performed using our own software written in Matlab (The Mathworks). Cell numbers of proliferating and quiescent NSPCs were assessed in separate plates grown in parallel using live Hoechst (5µg/ml, Invitrogen). 12 low magnification images from each triplicate were taken

and the number of nuclei counted using ImageJ. Measured malonyl-and acetyl-CoA values were normalized to the average cell number.

C13-incorporation and energy charge measurements

Proliferating and quiescent NSPCs were incubated for 24h with the corresponding medium containing 100μM C13-labelled palmitate (Cambridge Isotope Laboratories Inc.). Palmitate was coupled to BSA to achieve better cellular uptake. Metabolites were extracted with 800μL 80% methanol (at -80 °C), cells were scraped and the extracts were transferred to a 1.5ml tube. Next the extracts were centrifuged at 4°C for 15min at 20,000xg. The supernatant was dried using a vacuum centrifuge. To the dried fractions 25μL of a 2% methoxyamine hydrochloride solution (20mg dissolved in 1mL pyridine) was added and placed at 37°C for 90min. Then 75μl of N-tert-Butyldimethylsilyl-N-methyltrifluoro-acetamide with 1% N-tert-Butyldimethyl- chlorosilane (Sigma-Aldrich, Belgium) was added and the reaction was carried out for 30min at 60°C. Reaction mixtures were centrifuged for 15min at 20,000xg at 4°C in order to remove insolubilities, and the supernatant was transferred to a glass vial with conical insert (Agilent). GC-MS analyses were performed using an Agilent 7890A GC equipped with a HP-5 ms 5% Phenyl Methyl Silox (30 m - 0.25 mm i.d. - 0.25 μm; Agilent Technologies, Santa Clara, California, USA) capillary column, interfaced with a triple quadruple tandem mass spectrometer (Agilent 7000B, Agilent Technologies) operating under ionization by electron impact at 70eV. The injection port, interface and ion source temperatures were kept at 230°C.

Temperature of the quadrupoles was maintained at 150°C. The injection volume was 1µl, and samples were injected at 1:10 split ratio. Helium flow was kept constant at 1 ml/min. The temperature of the column started at 100 °C for 5 min and increased to 260 °C at 2°C/min. Next, a 40°C/min gradient was carried out until temp reached 300°C. After the gradient, the column was heated for another 3 min at 325°C. The GC-MS analyses were performed in Single Ion Monitoring (SIM) scanning for the isotopic pattern of metabolites.

For energy charge measurements (which is defined as following: (ATP+0.5*ADP)/(ATP+ADP+AMP)), metabolites of proliferating and quiescent NSPCs were extracted using 250 uL of an 80% methanol solution. Measurement of ATP, ADP and AMP levels was performed using a Dionex UltiMate 3000 LC System (Thermo Scientific) coupled to a Q Exactive Orbitrap mass spectrometer (Thermo Scientific) operated in negative mode. Practically, 30 µl of sample was injected on a SeQuant ZIC/ pHILIC Polymeric column (Merck Millipore). The gradient started with 20% of solvent B (2 mM Na-acetate in mqH_2O, pH 9.3) and 80% solvent A (95:5, acetonitrile:mqH_2O, containing 2 mM Na-acetate at pH 9.3) and remained at 20% B until 2 min post injection. Next, a linear gradient to 80% B was carried out until 29 min. At 38 min the gradient returned to 40% B followed by a decrease to 20% B at 42 min. The chromatography was stopped at 58 min. The flow was kept constant at 100 uL/min at the column was placed at 25°C throughout the analysis.

The MS operated both in full scan mode using a spray voltage of 3.2 kV, capillary temperature of 320°C, sheath gas at 10.0, auxiliary gas at 5.0. AGC target was

set at 1e6 using a resolution of 70.000, with a maximum IT of 100 ms. Data collection was performed using Xcalibur software (Thermo Scientific).

QUANTIFICATION AND STATISTICAL ANALYSIS

Quantifications were done as described in the METHOD DETAIL section.

Statistical analyses were performed with the software Prism 6 (GraphPad). Significance levels were set at $*p < 0.05$, $**p < 0.01$ and $***p < 0.001$.

The following tests were used:

Figure 1: A: unpaired t-test, two-tailed, n=3 coverslips per condition (10 images per coverlip), B: Wilcoxon matched-pairs signed Rank test against the hypothetical value 0. C: One-way-ANOVA followed by Holm-Sidak's multiple comparisons test, n=3 samples per condition. D and F: One-way-ANOVA followed by Holm-Sidak's multiple comparisons test, n=3 samples per condition. E: unpaired t-test, two-tailed, n=3 samples per condition. G: unpaired t-test, two-tailed, n=3 samples per condition

Figure 2: A: 2-way ANOVA with multiple comparisons, n=3 wells per condition (4-6 adjacent areas per well). B: unpaired t-test, two-tailed, n=3 samples per condition. C: One-way-ANOVA followed by Holm-Sidak's multiple comparisons test, n=3 samples per condition. D: unpaired t-test, two-tailed, n=3 samples per condition. F: One-way-ANOVA followed by Holm-Sidak's multiple comparisons

test, n=3 samples per condition. G: One-way-ANOVA followed by Holm-Sidak's multiple comparisons test, n=3 samples per condition.

Figure 3: B, C and D**:** paired t-test, two-tailed, n=3 mice (50-100 cells per mouse).

Figure 4: B, C and D: Contingency analysis, Chi^2-test, n=62 clones for S14iCre +/-; Cpt1a cKO wt/wt; R26YFP fl/wt, n=34 clones for S14iCre +/-; Cpt1a cKO fl/fl; R26YFP fl/wt.

Figure 5: A and B: One-way-ANOVA followed by Holm-Sidak's multiple comparisons test, n=3 coverslips per condition (10 images per coverlip).

Supplemental Figure 1: B: unpaired t-test, two-tailed, n=3 samples per condition. C: unpaired t-test, two-tailed, n=3 samples per condition. F: Wilcoxon matched-pairs signed Rank test against the hypothetical value 0. G: unpaired t-test, two-tailed, n=3 samples per condition.

Supplemental Figure 2: A: 2-way ANOVA with multiple comparisons, n=3 wells per condition (4-6 adjacent areas per well). B: One-way-ANOVA followed by Holm-Sidak's multiple comparisons test, n=3 samples per condition. C: One-way-ANOVA followed by Holm-Sidak's multiple comparisons test, n=3 coverslips per condition (10 images per coverslip). D: One-way-ANOVA followed by Holm-Sidak's multiple comparisons test, n=3 samples per condition.

Supplemental Figure 4: A, B and C: Contingency analysis, Chi^2-test, n=24 clones for S14iCre +/-; Cpt1a cKO wt/wt; R26YFP fl/wt, n=17 clones for S14iCre +/- ; Cpt1a cKO fl/fl; R26YFP fl/wt. D: grouped analysis, multiple t-tests, two tailed, n= 4 mice for S14iCre +/-; Cpt1a cKO wt/wt; R26YFP fl/wt, n=5 mice for

S14iCre +/- ; Cpt1a cKO fl/fl; R26YFP fl/wt. E: grouped analysis, multiple t-tests, two tailed, n= 3 mice for S14iCre +/-; Cpt1a cKO wt/wt; R26YFP fl/wt, n=7 mice for S14iCre +/- ; Cpt1a cKO fl/fl; R26YFP fl/wt. F: unpaired t-test, two tailed, n= 4 mice for S14iCre +/-; Cpt1a cKO wt/wt; R26YFP fl/wt, n=5 mice for S14iCre +/- ; Cpt1a cKO fl/fl; R26YFP fl/wt. G: unpaired t-test, two tailed, n= 3 mice for S14iCre +/-; Cpt1a cKO wt/wt; R26YFP fl/wt, n=7 mice for S14iCre +/- ; Cpt1a cKO fl/fl; R26YFP fl/wt. I: unpaired t-test, two tailed, n= 3 samples per condition. L: 2-way ANOVA followed by uncorrected Fisher's LSD, n=3 embryos (4-5 slices per animal) non-targeting shRNA, n=4 embryos (4-5 slices per animal) Cpt1a shRNA. M: unpaired t-test, two tailed, n=4 embryos (4-5 slices per animal) non-targeting shRNA, n=5 embryos (4-5 slices per animal) Cpt1a shRNA.

Supplemental Figure 5: B: Unpaired t-test, two tailed, n= 3 samples per condition, D: One-way-ANOVA followed by Holm-Sidak's multiple comparisons test, n=3 coverslips per condition (10 images per coverlip).

DATA AND SOFTWARE AVAILABILITY

The mass spectrometry proteomics data have been deposited to the ProteomeXchange Consortium via the PRIDE partner repository with the dataset identifier PXD005598

SUPPLEMENTAL INFORMATION REFERENCES

Asami, M., Pilz, G.A., Ninkovic, J., Godinho, L., Schroeder, T., Huttner, W.B., and Gotz, M. (2011). The role of Pax6 in regulating the orientation and mode of cell

division of progenitors in the mouse cerebral cortex. Development (Cambridge, England) *138*, 5067-5078.

Bonaguidi, M.A., Wheeler, M.A., Shapiro, J.S., Stadel, R.P., Sun, G.J., Ming, G.L., and Song, H. (2011). In Vivo Clonal Analysis Reveals Self-Renewing and Multipotent Adult Neural Stem Cell Characteristics. Cell.

Buescher, J.M., Moco, S., Sauer, U., and Zamboni, N. (2010). Ultrahigh performance liquid chromatography-tandem mass spectrometry method for fast and robust quantification of anionic and aromatic metabolites. Anal Chem *82*, 4403-4412.

Djouadi, F., Bonnefont, J.P., Munnich, A., and Bastin, J. (2003). Characterization of fatty acid oxidation in human muscle mitochondria and myoblasts. Mol Genet Metab *78*, 112-118.

Knobloch, M., Braun, S.M., Zurkirchen, L., von Schoultz, C., Zamboni, N., Arauzo-Bravo, M.J., Kovacs, W.J., Karalay, O., Suter, U., Machado, R.A.*, et al.* (2013). Metabolic control of adult neural stem cell activity by Fasn-dependent lipogenesis. Nature *493*, 226-230.

Martynoga, B., Mateo, J.L., Zhou, B., Andersen, J., Achimastou, A., Urban, N., van den Berg, D., Georgopoulou, D., Hadjur, S., Wittbrodt, J.*, et al.* (2013). Epigenomic enhancer annotation reveals a key role for NFIX in neural stem cell quiescence. Genes & development *27*, 1769-1786.

Mira, H., Andreu, Z., Suh, H., Lie, D.C., Jessberger, S., Consiglio, A., San Emeterio, J., Hortiguela, R., Marques-Torrejon, M.A., Nakashima, K.*, et al.* (2010). Signaling through BMPR-IA regulates quiescence and long-term activity of neural stem cells in the adult hippocampus. Cell Stem Cell *7*, 78-89.

Ray, J., and Gage, F.H. (2006). Differential properties of adult rat and mouse brain-derived neural stem/progenitor cells. Molecular and cellular neurosciences *31*, 560-573.

Schoors, S., Bruning, U., Missiaen, R., Queiroz, K.C., Borgers, G., Elia, I., Zecchin, A., Cantelmo, A.R., Christen, S., Goveia, J.*, et al.* (2015). Fatty acid carbon is essential for dNTP synthesis in endothelial cells. Nature *520*, 192-197.

Wisniewski, J.R., Zougman, A., Nagaraj, N., and Mann, M. (2009). Universal sample preparation method for proteome analysis. Nature methods *6*, 359-362.